Magma Fragmentation

Helge M. Gonnermann

Department of Earth Science, Rice University, Houston, Texas 77005;
email: helge.m.gonnermann@rice.edu

Annu. Rev. Earth Planet. Sci. 2015. 43:431–58

First published online as a Review in Advance on March 23, 2015

The *Annual Review of Earth and Planetary Sciences* is online at earth.annualreviews.org

This article's doi:
10.1146/annurev-earth-060614-105206

Keywords

magma, glass transition, brittle, viscoelastic, explosive, pyroclast

Abstract

Magma fragmentation is the breakup of a continuous volume of molten rock into discrete pieces, called pyroclasts. Because magma contains bubbles of compressible magmatic volatiles, decompression of low-viscosity magma leads to rapid expansion. The magma is torn into fragments, as it is stretched into hydrodynamically unstable sheets and filaments. If the magma is highly viscous, resistance to bubble growth will instead lead to excess gas pressure and the magma will deform viscoelastically by fracturing like a glassy solid, resulting in the formation of a violently expanding gas-pyroclast mixture. In either case, fragmentation represents the conversion of potential energy into the surface energy of the newly created fragments and the kinetic energy of the expanding gas-pyroclast mixture. If magma comes into contact with external water, the conversion of thermal energy will vaporize water and quench magma at the melt-water interface, thus creating dynamic stresses that cause fragmentation and the release of kinetic energy. Lastly, shear deformation of highly viscous magma may cause brittle fractures and release seismic energy.

1. INTRODUCTION

Pyroclasts: fragments of magma ejected during explosive eruptions: ash (<2 mm), lapilli (2–64 mm), and bombs (>64 mm)

Brittle fragmentation: material response above a critical stress by fracture and loss of continuity (cohesion)

Volcanic eruptions range widely in style and intensity. They may produce lava flows, pyroclastic material, or both. The process by which pyroclastic material is produced is referred to as magma fragmentation. It involves the breakup of a contiguous volume of magma into individual pieces. These fragments of magma, usually ejected into the air during explosive volcanic activity, are called pyroclasts. The mechanisms that govern magma fragmentation, the focus of this article, can be divided into four types: (*a*) brittle fragmentation, (*b*) fluid-dynamic breakup, (*c*) fragmentation by water-magma interaction, and (*d*) fragmentation by shear. The latter, however, may neither be a consequence of explosive volcanic activity nor necessarily result in the production of pyroclasts.

Throughout this article the term magma is meant to indicate a contiguous volume of molten rock—that is, silicate melt that may contain bubbles and/or crystals. The bubbles contain a supercritical fluid mixture, herein referred to as vapor or gas and primarily composed of H_2O, CO_2, and SO_2. At large depths and pressures magmatic volatiles are dissolved within the melt, but upon magma ascent their pressure-dependent solubility leads to exsolution by nucleating new bubbles and diffusion into existing bubbles. Upon fragmentation the magma becomes disrupted into individual fragments, thereby facilitating the release of magmatic gases from confining bubbles. The magma transitions from a contiguous melt phase with suspended bubbles to a mixture consisting of a contiguous gas phase and dispersed magma fragments. Depending on the type of eruption, this gas may be composed solely of magmatic volatiles or may include some proportion of external water that came into contact with the magma during ascent to the surface.

Magma fragmentation may occur at some depth beneath the surface, usually within the volcanic conduit and/or above the surface. As the pyroclasts are transported to, at, or above the surface, collisions between clasts result in additional fragmentation, termed secondary fragmentation. Upon deposition, pyroclastic material may form unconsolidated tephra deposits or become welded to form pyroclastic rock. In some cases welded pyroclastic deposits may be able to flow for some distance in a process termed rheomorphic flow. In eruptions of low-viscosity basaltic or carbonatitic magmas, fragmentation will produce pyroclastic material that remains fluid and can, upon deposition, form lava flows and lava lakes.

After reviewing some general aspects of explosive volcanism and magma vesiculation, I discuss the two fragmentation mechanisms inherent to so-called dry or magmatic eruptions: brittle fragmentation and fluid-dynamic breakup. Volcanic eruptions may also involve external water. If the presence of water is a dominant factor for an eruption, the eruption is termed hydromagmatic or phreatomagmatic. I discuss the associated fragmentation in a separate section. Explosions that involve heat and external water, but do not erupt magma, are called phreatic and are not included in this review. However, magma fragmentation by shear and secondary fragmentation are discussed, each in a separate section.

2. OVERVIEW OF EXPLOSIVE VOLCANISM

This brief overview of the different types of explosive volcanic activity (**Figure 1**) provides context for the subsequent discussion about fragmentation. An explosion, whatever its cause, is the consequence of a rapid increase in the volume of some confined material, which usually is gaseous and hence compressible in nature. It results in a high rate of transformation of stored energy into the kinetic energy of the rapidly expanding gas phase that carries with it fragments of the confining material, as well as into the surface energy of the newly created fragments. Most natural explosions are a consequence of volcanic processes. As magma rises from depth, the resultant reduction in pressure causes dissolved magmatic volatiles to exsolve by nucleation of new bubbles and diffusion into existing bubbles (**Figure 2**).

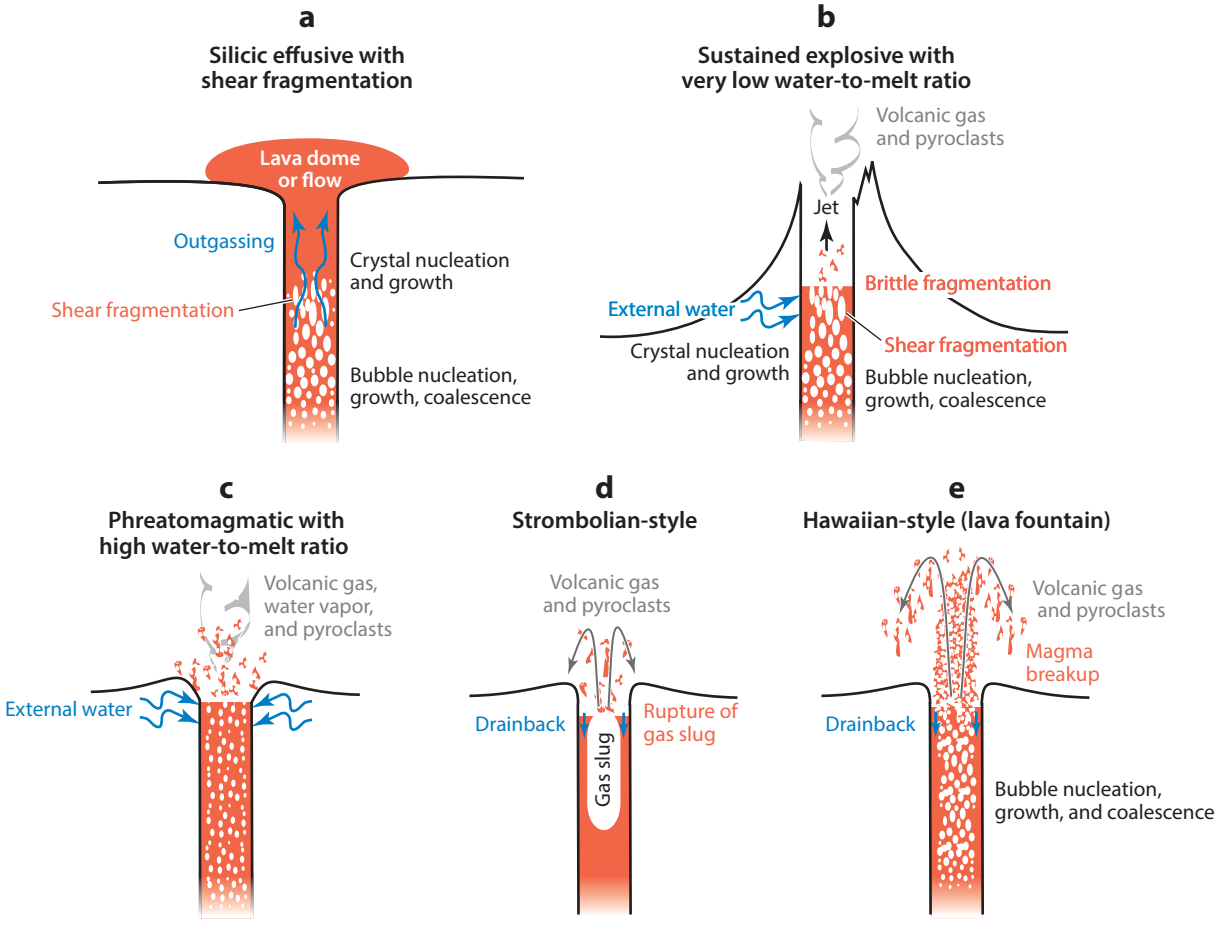

Figure 1

Schematic illustration of the different eruption styles considered in this article. (*a*) Effusive eruptions of silicic magma (high viscosity, low ascent rate). Magma may undergo shear fragmentation near conduit walls, thereby facilitating permeable gas flow. (*b*) Sustained explosive eruptions with brittle fragmentation due to gas overpressure. Some degree of magma-water interaction may also be possible. Upon fragmentation the flow changes from a viscous melt with suspended bubbles to a mixture of gas with suspended pyroclasts. (*c*) Phreatomagmatic explosive activity predominantly due to hydromagmatic fragmentation at high water-to-melt ratios. (*d*) Large gas slugs or bubble accumulations rise through a slowly ascending magma of low viscosity, producing Strombolian-style explosions upon rupture at the surface. (*e*) Magma breakup by fluid-dynamic stresses during Hawaiian-style eruptions, characterized by high ascent rates and sustained gas-pyroclast jets. Photographs illustrating the eruption styles depicted in panels *b*, *d*, and *e* are shown in **Figure 4**.

The supercritical H-C-O-S fluid is considerably more compressible than the surrounding melt (**Figure 3**), thus providing the potential for a rapid increase in volume during decompression. Explosive eruptions, caused by the release of magmatic volatiles as opposed to magma interaction with external water, are referred to as dry or magmatic eruptions. They include archetypal explosive eruption styles such as Strombolian, Hawaiian, Vulcanian, subplinian, Plinian, and ultraplinian. It should, however, be noted that there is a broad continuum of eruptive activity and many eruptions cannot simply be categorized in terms of such archetypical end-members (e.g., Houghton & Gonnermann 2008, Schipper et al. 2013, Castro et al. 2014). Thus, the following

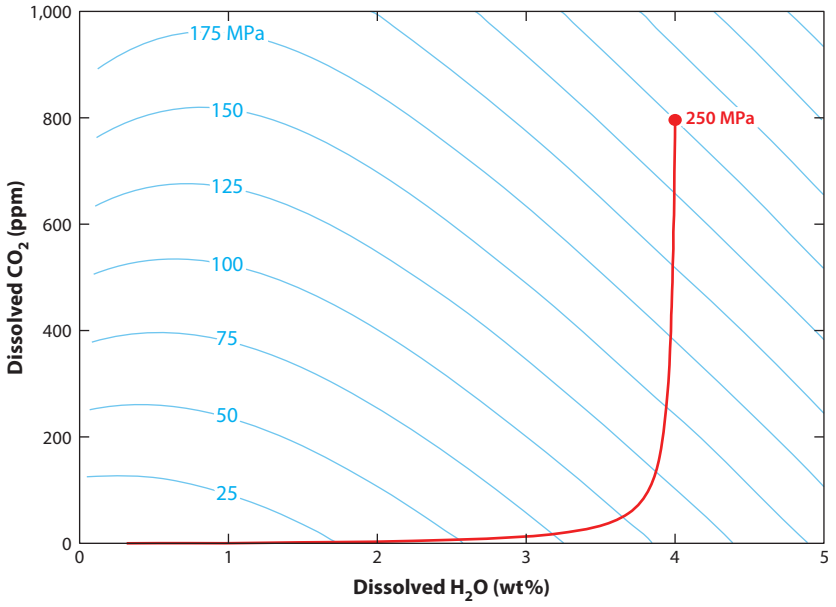

Figure 2

Solubility of H_2O and CO_2 in rhyolitic melt (Liu et al. 2005). Blue curves are pressure isopleths defined by the concentration of dissolved H_2O and CO_2 at the given pressure and temperature (875°C) and in equilibrium with an exsolved H_2O-CO_2 vapor mixture containing different proportions (mole fractions) of CO_2. For illustrative purposes, the red curve shows an equilibrium closed-system degassing trajectory starting at a pressure of 250 MPa.

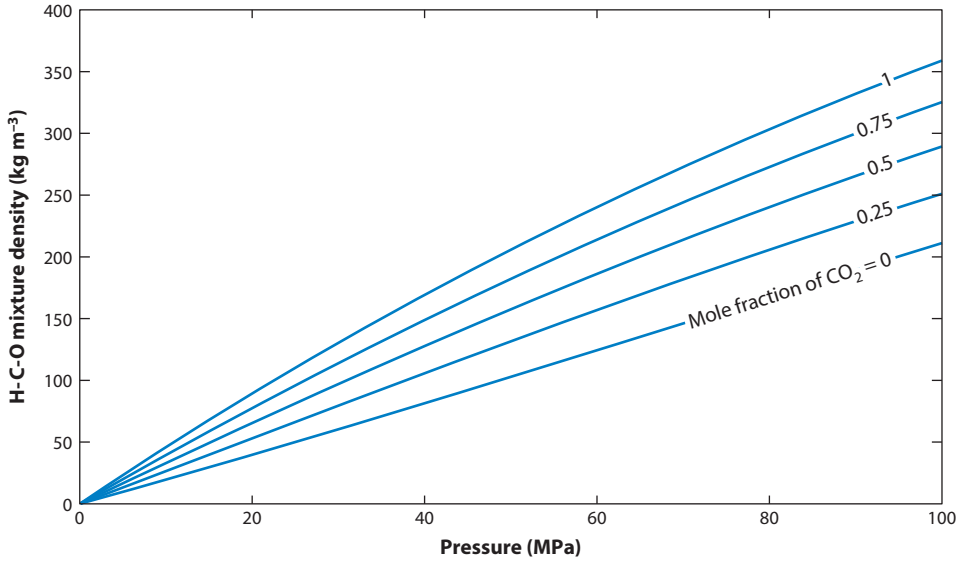

Figure 3

Density of a mixture of H_2O and CO_2 as a function of pressure, at a temperature of 850°C (Kerrick & Jacobs 1981). Individual curves represent CO_2 mole fractions of 0, 0.25, 0.5, 0.75, and 1.

review of eruption styles is primarily intended to highlight key characteristics of explosive eruptions and underlying processes.

2.1. Eruptions of Basaltic Magma

Volcanic jet: a collimated stream of magma and gas emanating from a vent into the air

Strombolian- and Hawaiian-style eruptions are associated with low-viscosity magma, usually basaltic in composition. Discrete Strombolian explosions are a consequence of the rise of large gas slugs or bubble agglomerations through a relatively stagnant magma column. They rupture once they reach the surface, and the surrounding magma fragments, due to stretching as the gas decompresses and expands (**Figure 4*a***) (Gerst et al. 2013, James et al. 2013).

In contrast, Hawaiian-style eruptions are characterized by hours to days of sustained eruptive activity in the form of a magma jet, also called a fire fountain, of up to hundreds of meters in height

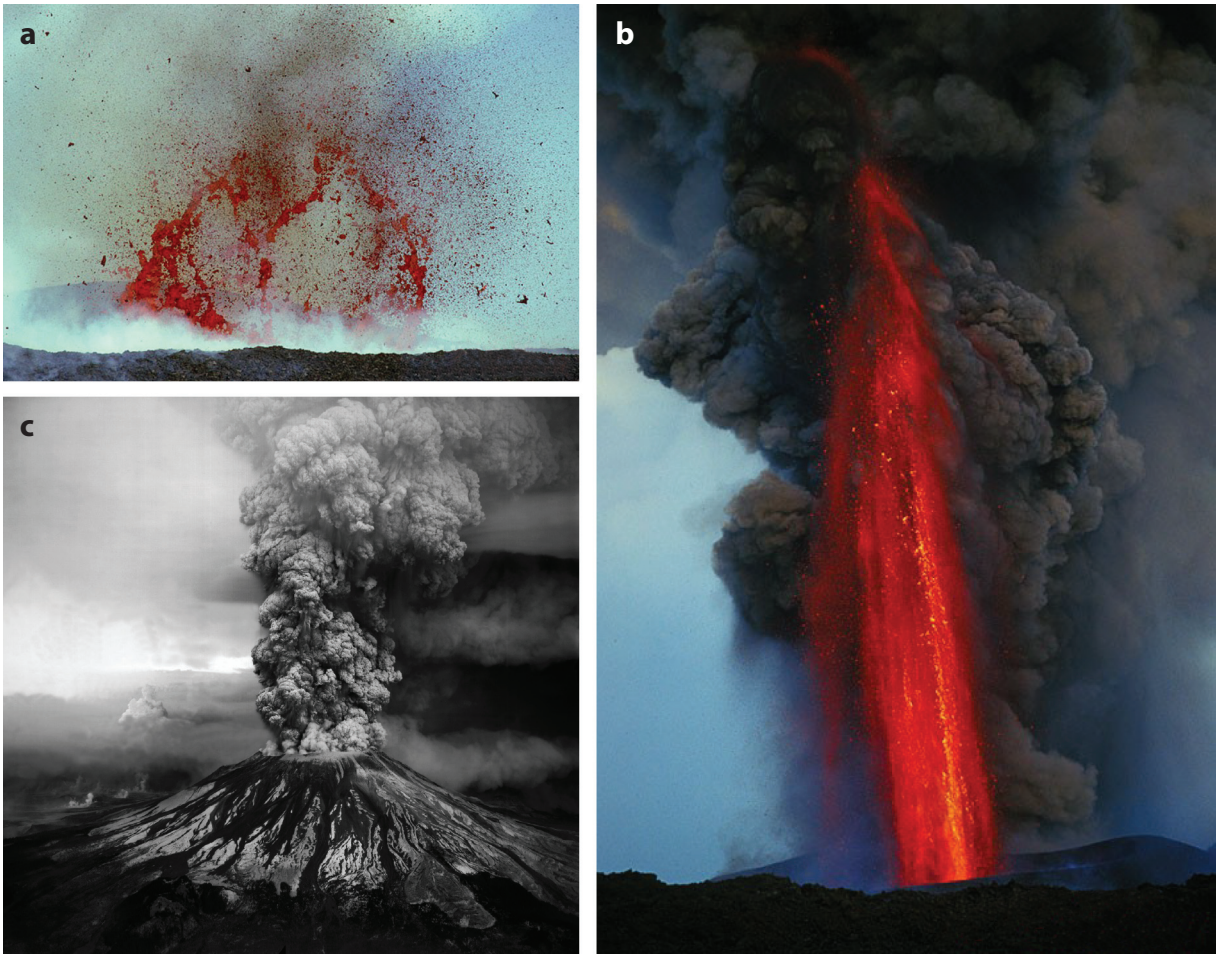

Figure 4

Photographs of magma fragmentation. (*a*) Bursting of a large bubble in weak Strombolian activity (Etna 2001; photograph by Tom Pfeiffer, **http://www.volcanodiscovery.com**; used with permission). (*b*) Hawaiian-style lava fountain (Etna 2001; photograph by Tom Pfeiffer, **http://www.volcanodiscovery.com**; used with permission). (*c*) Plinian eruption (Mount St. Helens 1980; photography by Robert Krimmel, US Geological Survey). Logos digitally deleted from panels *a* and *b*.

(**Figure 4*b***) (Houghton & Gonnermann 2008, Woods 2013). Magma fragmentation is, however, also a consequence of stretching by rapid expansion, as well as inertial forces and drag due to the high velocity of the gas within the fountain (Namiki & Manga 2008). Subplinian eruptions of basaltic magma are not uncommon (e.g., Branca & Del Carlo 2005), and whether they are a more intense form of Hawaiian activity may be debatable (Houghton & Gonnermann 2008). Similarly, the fragmentation mechanism during basaltic Plinian eruptions, of which few are known, remains controversial (Giordano & Dingwell 2003b, Goepfert & Gardner 2010).

Viscoelasticity: the capacity of a material to undergo recoverable elastic deformation on short timescales and behave viscously on long timescales

Elasticity: the ability of a body to return to its initial shape and size after a deforming stress is removed

2.2. Eruptions of Silicic Magma

Vulcanian- and Plinian-style eruptions are predominantly associated with magma of high viscosity (Eichelberger 1995), such as dacite and rhyolite. Vulcanian eruptions are short-lived explosions, caused by the sudden decompression of stagnant magma within the volcanic conduit. This is usually triggered by the disruption of a highly viscous magma plug within the uppermost part of the conduit and/or the collapse of an overlying magma dome. Sudden decompression results in brittle magma fragmentation and a single or a sequence of discrete explosions, which last for seconds to minutes and produce a buoyant eruption column (Clarke 2013).

Plinian-style eruptions, including subplinian and ultraplinian, are characterized by sustained explosive activity lasting for hours or days and producing 10–50-km-tall pyroclastic eruption columns (**Figure 4*c***) (Woods 2013). Magma fragmentation is thought to occur by gas overpressure of bubbles within a highly viscous magma, which fragments as a brittle solid at some depth within the volcanic conduit (Dingwell 1996, Papale 1999, Gonnermann & Manga 2007).

2.3. Eruptions Involving External Water

Explosive eruptions may include both magmatic and phreatomagmatic components. Furthermore, phreatic explosions may precede magmatic or phreatomagmatic eruptions. During phreatic eruptions, magma provides heat, which causes groundwater or surface water to flash to steam. The resultant rapid increase in volume creates an explosion of steam, water, magmatic gases, and rock fragments of variable size. Phreatic eruptions may produce low-relief craters and deposits consisting of fragmented country rock rather than fragmented magma.

In contrast, phreatomagmatic eruptions (e.g., Self & Sparks 1978, Sheridan & Wohletz 1983, Houghton et al. 2000b, White & Houghton 2000) involve magma plus external water. The rapid transfer of heat at the melt-water interface causes water to flash to steam, as well as causing rapid quenching of melt. The ensuing explosions may also fracture country rock, and phreatomagmatic deposits typically contain large proportions of resultant lithic fragments.

3. GLASS TRANSITION AND BRITTLE FRAGMENTATION

Brittle magma fragmentation requires that the melt, a viscoelastic material, responds to an applied stress in a predominantly elastic manner. This is the case for highly polymerized melts, if they are subjected to a sufficiently large stress. The glass transition defines the conditions of temperature and deformation rate under which the deformation changes from viscous to elastic, with recoverable elastic deformation at small strain and brittle failure at large strain (Dingwell 1996).

Silicate melts are composed of a disordered network of interconnected SiO_4 tetrahedra whose average molecular structure is in a dynamic equilibrium, due to the spontaneous breaking and remaking of Si–O bonds. This process is called structural relaxation and facilitates rearrangements of the molecular structure without disrupting it. Under an applied stress, molecular

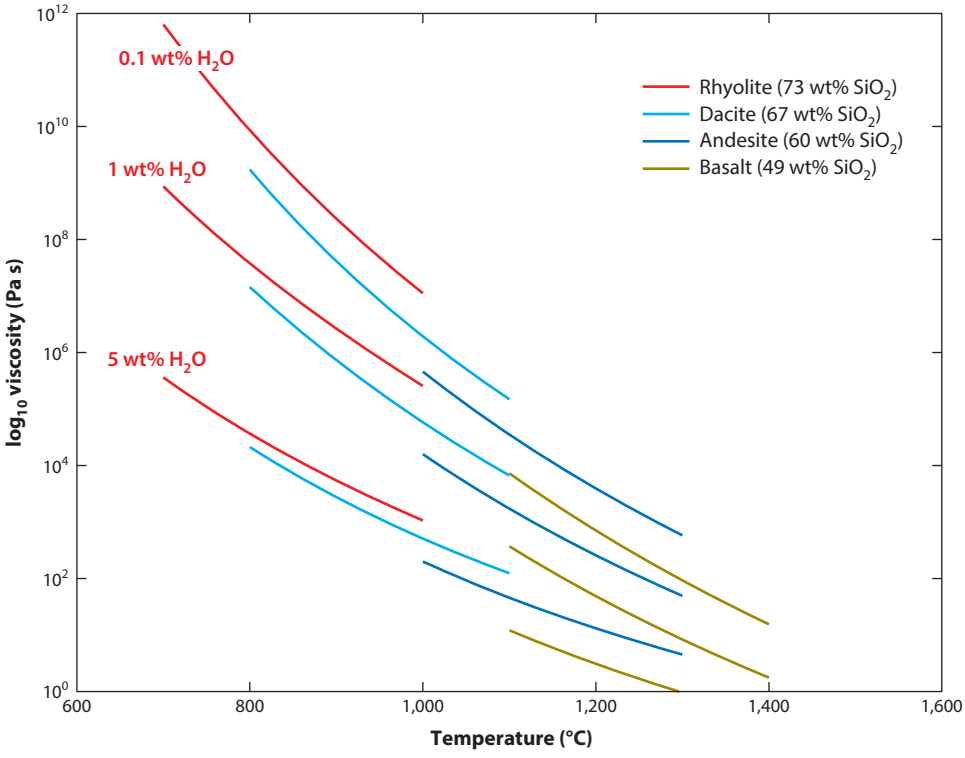

Figure 5

Viscosity as a function of temperature for natural silicate melts (Hui & Zhang 2007). Each composition is plotted for a range of typical eruptive temperatures. Viscosity decreases with temperature and dissolved water content, but increases with SiO_2 content. Furthermore, the dependence of viscosity on dissolved water increases with SiO_2.

rearrangements toward a state of structural relaxation result in irreversible ductile or viscous deformation (Moynihan 1995). The degree of structural cross-linking is characterized by the number of nonbridging oxygens per silicon tetrahedron (NBO/T) and affects melt viscosity, the constant of proportionality between strain rate and applied stress. Because NBO/T increases with silica content, viscosity decreases from silicic to mafic melts (Giordano & Dingwell 2003a). Furthermore, NBO/T decreases with dissolved water content, as a result of the dissociation of molecular water. Consequently, viscosity increases substantially as water exsolves, especially for high-silica (Hui & Zhang 2007). The rate of structural relaxation also increases with temperature, resulting in a decrease in viscosity as temperature increases, all else being equal (**Figure 5**).

If silicate melts are subjected to sufficiently large stress over a short duration, deformation may be mostly accommodated by reversible changes in molecular bond lengths and angles—in other words, by elastic deformation at small strain. In fact, over some range of stress the melt behaves approximately as a linear viscoelastic material. At sufficiently high stress, however, large strain deformation causes bonds within the silicate network to break, resulting in a decrease in apparent viscosity. This non-Newtonian behavior is known as shear thinning. Upon sufficiently long application of such high stress, the melt structure will be disrupted due to its inability to relax on the timescale of the deformation, resulting in brittle failure (e.g., Dingwell & Webb 1989; Webb & Dingwell 1990a,b).

Ductile deformation: response of a solid material to tensile stress by flowing mesoscopically like a viscous fluid with strain distributed throughout

Viscous deformation: nonreversible deformation of a fluid in response to an applied stress; Newtonian if stress and strain rate are linearly related

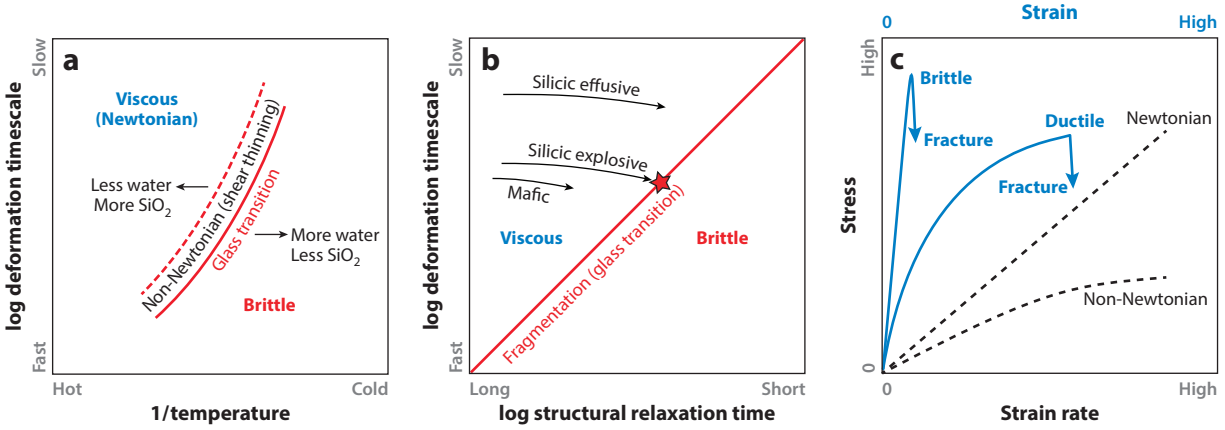

Figure 6

(*a*) Schematic diagram of the glass transition in time versus reciprocal temperature space (Dingwell 1996). Melt composition, temperature, and dissolved water content determine viscosity and, hence, the structural relaxation time. The melt deforms as a Newtonian viscous liquid if deformation rates are slower than $\sim 10^{-3.5} G/\eta_r$. At deformation rates $\gtrsim 10^{-2} G/\eta_r$, the flow becomes non-Newtonian and the response will be elastic at low strain and brittle failure at high strain. (*b*) Schematic diagram illustrating idealized hypothetical ascent paths for silicic and mafic magmas. During ascent magma degasses, which increases viscosity and decreases the structural relaxation time. Although deformation rates may not change by much, the magma approaches the glass transition and brittle fragmentation as it loses water. If the magma ascends slowly, it may never intersect the glass transition, because deformation rates are too slow. In contrast, even rapidly ascending mafic magma will not intersect the glass transition, because its structural relaxation time remains too large. (*c*) Schematic curves of stress versus strain (*solid blue lines*) and stress versus strain rate (*dashed black lines*). Silicate melts above the glass transition temperature deform as a Newtonian fluid at low strain rates and as a non-Newtonian (shear thinning) fluid at high strain rates. Below the glass transition they deform in a brittle manner by fracturing. Also shown is the behavior of a ductile solid.

The relaxation timescale can be estimated from the Maxwell relation $\tau_r = \eta_r/G$, where τ_r is the Maxwell time, η_r is the melt viscosity at low strain rates and $G \sim 10^{10}$ Pa is the shear modulus (Dingwell & Webb 1989, Webb & Dingwell 1990b, Dingwell 1997). Shear-thinning behavior occurs at strain rates approximately 3 ± 0.5 orders of magnitude lower than the relaxation rate τ_r^{-1}, whereas the transition to viscoelastic behavior occurs at strain rates of approximately 2 orders of magnitude below τ_r^{-1}. This transition between viscous or ductile and elastic or brittle behavior is the glass transition (**Figure 6**) (Dingwell 1996). Once the magma intersects the glass transition, fragmentation can be treated within the conceptual framework of fracture mechanics. In other words, at or beyond the glass transition high strain and strain rates prevent structural relaxation and the molecular structure of the magma is disrupted, resulting at the macroscopic scale in brittle fracturing. Numerical modeling suggests that magma expansion during eruption, due to volatile exsolution and decompression, can result in extensional strain rates sufficiently large to intersect the glass transition (Papale 1999).

Silicic melt: melt with >63 wt% SiO_2, usually dacitic or rhyolitic in composition and high in viscosity

Mafic melt: melt with 45–52 wt% SiO_2, usually basaltic in composition and low in viscosity

Maxwell time: the characteristic time over which stress decays after deformation of a viscoelastic material

4. ASCENT OF HIGH-VISCOSITY MAGMA

4.1. Conduit Flow

The pressure of ascending magma must decrease, mostly because of the hydrostatic pressure of the overlying magma and the pressure loss required to balance viscous stresses, also referred to as wall friction (Wilson 1999). In the simplest sense, for magma to erupt at steady conditions, the pressure within the chamber has to balance or exceed the integrated pressure loss within the

conduit (e.g., Wilson et al. 1980, Mastin 2002):

$$p_c - p_v = \int_c^v \left(-\rho g - f\frac{\rho u^2}{a} + \frac{\rho u^2}{a^2}\frac{da^2}{dz} + u^2\frac{d\rho}{dz} \right) dz. \quad (1)$$

Here subscripts c and v denote the chamber and vent, respectively. Furthermore, the conduit radius, a, the ascent velocity, u, and the magma density, ρ, are all functions of the vertical coordinate z. The first term on the right hand side of Equation 1 is the hydrostatic or, rather, magmastatic pressure loss, whereas the second term is the frictional pressure loss, with $f \approx f_0 + 8\eta/\rho ua$ and $f_0 \sim 0.001$–0.01, where η is the magma viscosity, which principally depends on the viscosity of the silicate melt, η_m. Near the conduit walls, heating by viscous dissipation (e.g., Mastin 2005) and the presence of bubbles or crystals (Mader et al. 2013) have the potential to affect η and, hence, f. In addition, shear fragmentation (Goto 1999, Gonnermann & Manga 2003) would also affect f. The third and fourth terms are due to magma acceleration, which in the case of a constant discharge rate may arise from changes in conduit radius, as well as from volatile exsolution and expansion, which decrease magma density.

Assuming the conduit radius does not change drastically with depth, the pressure loss due to friction and acceleration is small, relative to magmastatic pressure, especially if u is small. Moreover, magmastatic pressure tends to be smaller than lithostatic pressure, because magma density decreases as a consequence of volatile exsolution. Therefore, values of p_c, which may exceed lithostatic pressure by up to 10 MPa (Jellinek & DePaolo 2003) or more, can result in the slow (effusive) eruption of high-viscosity magma. As u increases, the frictional pressure loss, especially as the magma becomes more viscous due to water exsolution, can become so large that reasonable values of p_c are insufficient to drive the magma to the surface, unless the magma fragments at some depth z_f. If this is this case, the gases are abruptly released from confining bubbles and expand. Not only does the resultant decrease in density of the gas-pyroclast mixture, relative to the density of the bubbly magma, reduce the magmastatic pressure above z_f, but the low viscosity of the gas-pyroclast mixture also drastically reduces the frictional pressure loss above z_f (**Figure 7**) (Dobran 1992, Mader 1998, Papale 2001, Dufek & Bergantz 2005, Koyaguchi 2005). Fragmentation of high-viscosity magma thus may not only require rapid magma ascent rates, it may also be a necessary condition for high-viscosity magma to erupt at high discharge rates.

4.2. Bubble Overpressure

Although the density and viscosity of magmatic vapor are much smaller than the density of melt (**Figure 3**), buoyant bubble rise is resisted by viscous drag of the surrounding melt. The relative velocity between bubbles and melt is approximately equal to $R^2 g \Delta\rho/(3\eta_m)$ (Batchelor 1967), where R is bubble radius, η_m is melt viscosity, and $\Delta\rho \sim 10^3$ kg m^{-3} is the density difference between vapor and melt. In silicic magmas, this relative velocity tends to be negligibly small and bubbles are passively transported with the melt, although they may grow in size.

Decreasing pressure of the ascending magma will lower the volatile solubility (**Figure 2**), resulting in diffusion of volatiles into bubbles, where they are of lower density, which will decrease further during decompression (**Figure 3**). The resultant bubble growth is resisted by viscous deformation of the melt. Assuming spherical bubbles, uniform packing geometry, and negligible inertial stress because of the large viscosity of silicate melt, bubble growth can be described by a simplified version of the Rayleigh–Plesset equation (Proussevitch et al. 1993, Lensky et al. 2001):

$$\Delta p = p_g - p = \frac{2\gamma_s}{R} + 4\eta_m\frac{\dot{R}}{R}. \quad (2)$$

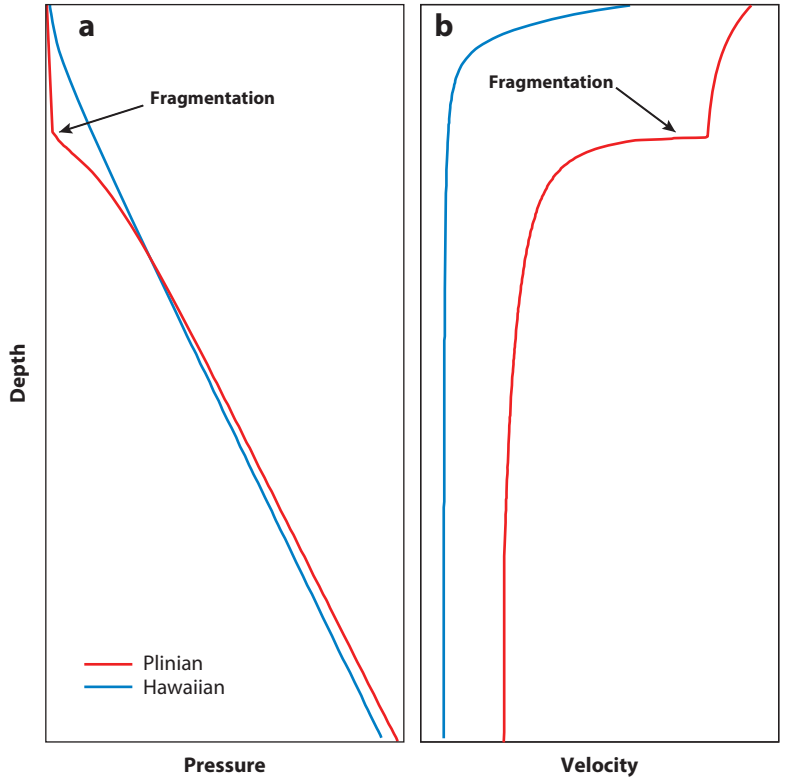

Figure 7

Illustrative examples of (*a*) magma pressure and (*b*) magma velocity, both as a function of depth, for a Hawaiian-style eruption of basaltic magma (*solid blue lines*) and for a Plinian-style eruption of rhyolitic magma (*solid red lines*). For the basaltic magma frictional pressure loss may be smaller than the magmastatic change in pressure. For the rhyolitic magma frictional pressure loss becomes much larger than the magmastatic change in pressure, once appreciable amounts of water exsolve. Without fragmentation and the resultant low-viscosity gas-pyroclast mixture, the eruption of highly viscous magma at high velocities is difficult.

Here p is the magma pressure, p_g the gas pressure inside the bubble, S the half-distance between adjacent bubbles, $\dot{R}$ the bubble growth rate, and $\gamma_s \sim 0.1\ \mathrm{N\ m^{-1}}$ the surface tension between vapor and melt. Furthermore, η_m is the effective melt viscosity, which accounts for the nonuniform melt viscosity caused by water diffusion and the resultant gradients in dissolved water. The first term on the right hand side is the Laplace pressure, the excess pressure inside a static bubble, which is due to surface tension and is unlikely to exceed $\sim 10^5$ Pa under typical magmatic conditions (i.e., $R \gtrsim 10^{-6}$ m).

The last term in Equation 2 is the viscous stress. For a decompression rate of $\dot{p}$, the characteristic decompression timescale is $\tau_p \sim \Delta p / \dot{p}$. If τ_p is much smaller than the viscous timescale for bubble growth, $\tau_\eta \sim \eta_m / \Delta p$, then there is insufficient time for the vapor inside bubbles to expand and Δp can become much larger than the Laplace pressure. Such buildup of overpressure is favored if η_m is large, in which case frictional pressure loss within the conduit is also large, causing $\dot{p}$ to be large. The magnitude of $\dot{p}$ can be estimated from the product of u and the frictional pressure gradient in Equation 1 as $\dot{p} \sim \rho u^3 f / a$, where below fragmentation $f \approx 8\eta / \rho u a$ tends to be a

reasonable approximation. Furthermore, accounting for a reduction in magma viscosity of up to approximately 1 order of magnitude, relative to the melt viscosity, η_m, due to the presence of bubbles at high capillary numbers (Mader et al. 2013), one obtains $\dot{p} \sim u^2\eta_m/a^2$. Consequently, the condition $\tau_p \ll \tau_\eta$ is equivalent to $\Delta p \ll \eta_m u/a$. This is the viscous limit of bubble growth, which is most likely reached once the concentration of dissolved water reaches less than ~1 wt% (e.g., Sparks 1978).

Overpressure is thought to be primarily associated with the rapid ascent of magma during subplinian and Plinian eruptions. However, the condition $\tau_p \ll \tau_\eta$ is also met during the rapid decompression of more or less stationary magma, for example, associated with unloading during sector collapse, as occurred during the 1980 eruption of Mount St. Helens, Washington. Similarly, dome collapse or the disruption of a shallow magma plug may also result in rapid unloading, as has been occurring, for example, during the eruption of the Soufrière Hills volcano, Montserrat.

4.3. Fragmentation by Bubble Overpressure

Brittle fragmentation in bubbly viscoelastic fluids that are undergoing abrupt decompression has been observed experimentally (Ichihara et al. 2002, Namiki & Manga 2005). Similarly, brittle fragmentation of vesicular magma has been reproduced experimentally by confining and heating porous volcanic rock samples within a pressurized shock tube and then decompressing it near-instantaneously by rupturing a diaphragm at one end (Alidibirov & Dingwell 1996; Martel et al. 2000, 2001; Spieler et al. 2004; Kueppers et al. 2006b; Scheu et al. 2006; Mueller et al. 2008). A decompression wave propagates into the sample, and it fragments if the change in pressure exceeds a threshold of approximately σ_t/ϕ, where $\sigma_t \approx 10^6$ Pa is the tensile strength of the melt and ϕ is the volume fraction of vesicles (**Figure 8**).

This dependence of the fragmentation threshold on ϕ derives from the geometrical relationships of stress distribution within the melt surrounding bubbles (e.g., Zhang 1998, 1999; Koyaguchi & Mitani 2005; Koyaguchi et al. 2008). The value of σ_t has also been estimated from fiber elongation studies, obtaining values of $\sim 10^8$ Pa (Webb & Dingwell 1990b), which are considerably higher than those obtained from shock tube experiments. A possible explanation for this discrepancy is the presence of microcracks within bubble walls (Romano et al. 1996). As water diffuses from the melt into bubbles, the resultant concentration gradients result in viscosity gradients (Lensky et al. 2001) and volume stresses, due to the dependence of molar melt volume on dissolved water content (Mungall et al. 1996). Because the samples used in the shock tube experiments were cooled and solidified prior to reheating and decompression, they presumably contained such microcracks. In contrast, the formation of microcracks in erupting magmas is contingent on the development of volume stresses that locally exceed the tensile strength of the melt on timescales that are shorter than the relaxation time. Stress localization at the tips of such microcracks, if they indeed exist, should then decrease the effective tensile strength of erupting magmas to $\sigma_t \sim 10^6$ Pa (Alidibirov 1994, Zhang 1999, Spieler et al. 2004, Koyaguchi et al. 2008).

Fragmentation in shock tube experiments proceeds via the formation of brittle fractures that propagate layer by layer into the sample, producing fragments that range in size from tens of micrometers to centimeters (Kueppers et al. 2006a,b). It is envisaged that magma fragments in this manner during sustained explosive eruptions, by ascending rapidly into a region of steep pressure gradients, which in turn are a consequence of acceleration due to bubble nucleation and growth as well as the resultant increase in viscosity (Papale 1999, 2001; Koyaguchi et al. 2008). Consequently, frictional pressure losses increase while the melt relaxation rate decreases. The magma thus rises monotonically toward conditions that favor brittle fragmentation (**Figure 7**).

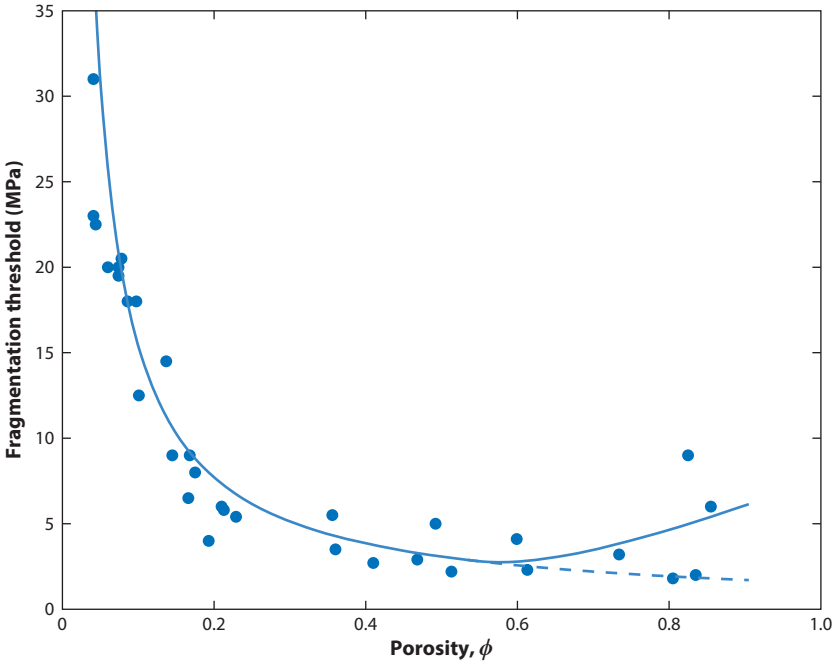

Figure 8

Pressure drop as a function of the sample porosity, ϕ, at which 850°C hot volcanic rock samples of various compositions fragmented upon abrupt decompression (Spieler et al. 2004). Also shown are the empirical threshold of σ_t/ϕ (*dashed curve*), where $\sigma_t = 1.54 \times 10^6$ Pa, and the empirical threshold that accounts for pressure dissipation by permeable gas flow (*solid curve*), given by $[(8.21 \times 10^{11}\text{Pa m}^{-1})\sqrt{k} + \sigma_t]/\phi$ (Mueller et al. 2008), where permeability is based on measured values in silicic Plinian pyroclasts and is given by $k = (9 \times 10^{-10}\ \text{m}^2)(\phi - \phi_c)^n$, with a percolation threshold of $\phi_c = 0.55$ and $n = 3.5$.

In other words, ϕ, η_m, and u all increase, driving the magma toward $\eta_m u/a \gg \sigma_t/\phi$, which is equivalent to a Deborah number criterion, $\tau_r \gg \tau_p$, for brittle fragmentation. In contrast, during unloading events and Vulcanian eruptions, the decompression wave propagates downward into a relatively stagnant and degassed magma of high viscosity, but also with $\tau_\eta \gg \tau_p$ and $\tau_r \gg \tau_p$ (Clarke 2013).

4.4. The Role of Magma Permeability

An important factor in modulating brittle magma fragmentation may be the development of interconnected networks of bubbles through coalescence. They render the erupting magma permeable, facilitating the outgassing of exsolved volatiles and dissipation of overpressure (Eichelberger et al. 1986; Blower 2001; Rust & Cashman 2004, 2011; Wright et al. 2009). Consequently, fragmentation of permeable magma requires an increase in fragmentation overpressure of approximately 10^{12} Pa m$^{-1}\sqrt{k}/\phi$ relative to impermeable magma, where k is the Darcian permeability (**Figure 8**) (Mueller et al. 2008). To what extent this modulates explosive activity remains a subject of debate (Nguyen et al. 2014). By the same token, permeable magma does not need to fragment to ash-sized particles in order to release the compressed vapor from within bubbles (Klug & Cashman 1996) and transition to a low-viscosity gas-pyroclast mixture.

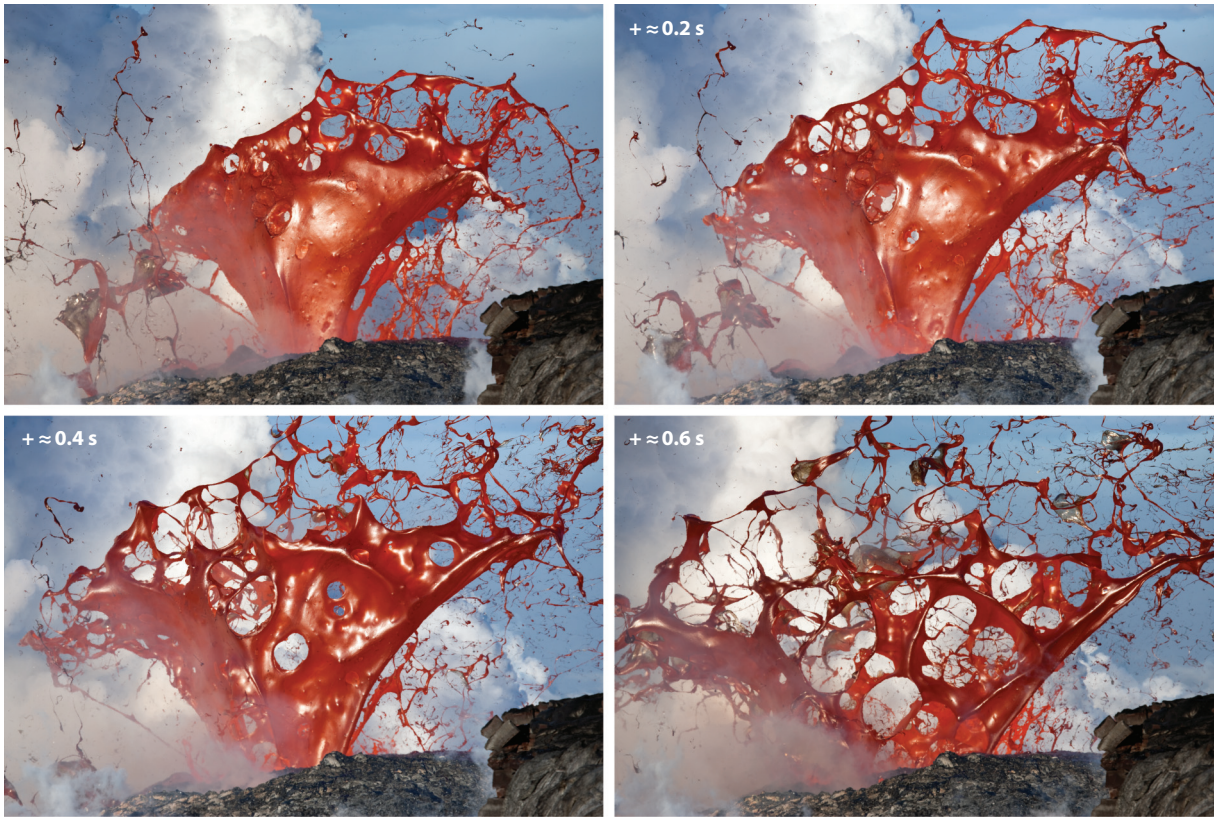

Figure 9

Fluid-dynamic breakup of basaltic magma by an expanding vapor bubble of about 10–30 m in diameter at Kilauea volcano, Hawaii. The time interval between individual frames is approximately 0.2 s. The magma becomes stretched into a sheet that breaks up into filaments, which in turn break up into pyroclasts. Photographs by Bruce Omori, Extreme Exposure; used with permission.

5. FLUID-DYNAMIC BREAKUP

5.1. The Mechanics of Breakup

In volcanic eruptions of low-viscosity magmas, such as basalt, fragmentation occurs not by intersection with the glass transition, but rather by breakup in the liquid state through hydrodynamic stresses and instabilities. This is a common phenomenon of everyday life, such as, for example, the breakup of a jet of water or the droplets generated from bursting bubbles. It involves a change in topology from a compact macroscopic volume into sheets and filaments. The latter then break apart into smaller fragments, either because of capillary instability to along-axis variations in thickness or because of pinch-off when stretched to some critical thickness (**Figure 9**).

Capillary instabilities arise because the local pressure inside a liquid filament is greater than the pressure of the surrounding gas or air, by an amount that is inversely proportional to the local radius of curvature of the interface. Because the smallest radius of curvature corresponds to the thinnest part of the filament, there will be an axial pressure gradient, causing flow from thinner to thicker parts. Once a segment reaches a thickness of the order of 1 μm (Kowalewski 1996), it pinches off and retracts to form a more compact volume with lower surface energy (Eggers 1993,

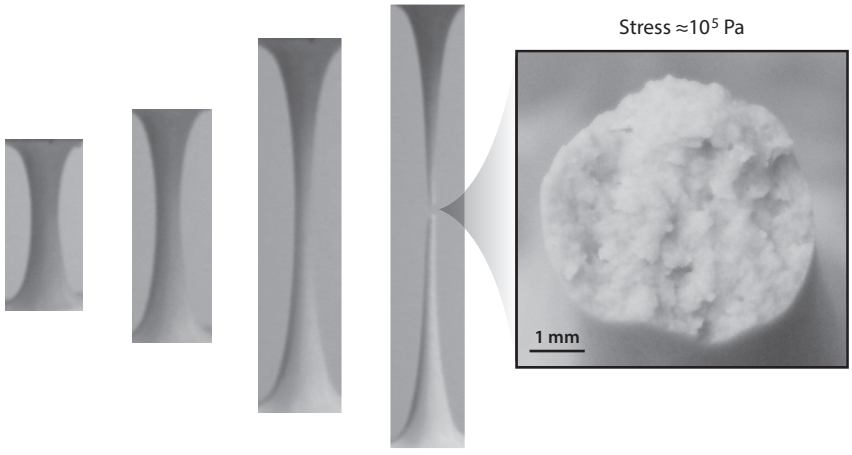

Figure 10

Example of fracture of a concentrated suspension of solid particles in a Newtonian liquid, potentially analogous to fragmentation of highly crystal-rich magmas. The material is composed of 5-μm-diameter spherical particles suspended in silicone oil of 100 Pa s viscosity and 60% particles by volume fraction. The sample deforms in a ductile manner by necking until it undergoes brittle fracture at a stress of approximately 10^5 Pa (Moitra et al. 2010).

Shikhmurzaev 2000, Israelachvili 2011). Bubbles or particles can significantly affect the breakup of liquid sheets and filaments (e.g., Huisman et al. 2012, Miskin & Jaeger 2012, Villermaux 2012), resulting, for example, in filaments that break at larger diameters or undergo ductile fracture (**Figure 10**) (Smith et al. 2010).

Filament formation, and ultimately breakup, can be dominated by capillary or viscous forces. The capillary-dominated characteristic breakup time is $\tau_{cap} \sim \sqrt{\rho d/\gamma_s}$, where d is the diameter. If viscous forces dominate, then breakup is slowed and the characteristic timescale is instead $\tau_{vis} \sim \eta d/\gamma_s$. The ratio of these two timescales is the Ohnesorge number, $Oh = \tau_{vis}/\tau_{cap}$ (Villermaux 2012). For magmas, breakup is dominated by viscous forces, because $Oh \gg 1$. If the filament is being stretched in the axial direction at an elongation rate of τ_{str}^{-1}, the instability is suppressed if $\tau_{str} < \max[\tau_{vis}, \tau_{cap}]$, although it will still break up, once a critical thickness is reached.

In many situations, such as a liquid drop within a stream of air, the liquid will first deform into a flattened shape with a toroidal rim that contains most of the liquid volume. As the sheet becomes stretched, it eventually ruptures, and the filament-like rim becomes corrugated and breaks up into drops. These drops may themselves break up into smaller drops, in what can be considered a cascade of breakups (Villermaux 2007). A key parameter associated with the resultant fragment (drop) size is the aerodynamic Weber number, $We_g \sim \rho_g u_{gm}^2 l/\gamma_s$, where ρ_g represents the density of the surrounding gas, u_{gm} is the difference in velocity between the surrounding gas and the drop, and l is the drop diameter. The Weber number represents the ratio of the stress due to drag between gas and liquid, $\rho_g u_{gm}^2$, which is essentially a stagnation pressure that will deform the drop, and the capillary pressure, γ_s/l, which tends to restore the drop to spherical shape. Existing scaling relationships of fragment (drop) size distribution and We_g are summarized by Villermaux (2007) and Eggers & Villermaux (2008).

In turbulent jets, filaments and drops are also formed as a consequence of shear at the interface between the liquid and the surrounding air or gas. The dynamics of jet disintegration depend on a Reynolds number and a Weber number, each of which is based on the liquid viscosity and

on the relative velocity between liquid and gas (Lin & Reitz 1998, Villermaux 2007, Eggers & Villermaux 2008). The fragmentation process becomes increasingly effective at disrupting the jet as inertial forces increase relative to viscous and capillary forces—in other words, as Reynolds and Weber numbers increase. For magma it is reasonable to expect that the topology of the gas-melt mixture, due to the presence of bubbles, plays a significant role during deformation into filaments and subsequent breakup (Dombrowski & Fraser 1954), as illustrated in **Figure 9**.

5.2. Breakup During Explosive Eruptions

Mafic magmas are the most ubiquitous magmas on Earth and many other planetary bodies. They are of lower viscosity than silicic magmas and have weaker dependence of viscosity on water content (**Figure 5**). Hence, frictional pressure losses are much smaller than for silicic magmas ($\lesssim 10^6$ Pa), and magmastatic pressure losses dominate during eruptive ascent, even at eruption velocities of $\sim$10 m s^{-1} (**Figure 7**). Moreover, bubble growth is not impeded by melt viscosity, and comparatively little overpressure builds up. Because the structural relaxation timescale depends on melt viscosity, mafic melts do not intersect the glass transition and are unlikely to fragment in a brittle manner, even at high ascent rates. Instead they fragment by fluid-dynamic breakup.

An important consideration is the dynamics and the topology of the magma-gas mixture. Bubbles are mobile within the ascending magma, potentially resulting in high rates of bubble coalescence. As a consequence, the ascent of low-viscosity magma may involve different flow regimes at shallow depth, where the volume fraction of exsolved volatiles can reach large values. Gas-liquid flow regimes depend on the volumetric flow rate per unit cross-sectional area of gas and liquid, also referred to as the superficial velocity (Schlegel et al. 2014). At low superficial gas velocities and/or high superficial liquid velocities, bubbles are dispersed throughout the liquid and the flow regime is called bubbly. At higher superficial gas velocities, the gas-liquid topology can become highly complex and dynamic, as liquid sheets and films that separate individual bubbles deform and rupture, resulting in transitions to slug, churn, annular, and mist flow. Although it is controversial whether such transitions take place during volcanic eruptions (Wilson 1999, Parfitt 2004), it stands to reason that the transition of low-viscosity magma into a gas-pyroclast mixture involves a complex spectrum of fluid dynamics, with the breakup of sheets and filaments playing a central role.

5.2.1. Magma jets: Hawaiian. For sustained explosive eruptions of low-viscosity magma, such as Hawaiian-style eruptions, the flow within the conduit will be turbulent. If the pre-eruptive exsolved gas fraction is small, then the magma begins its ascent almost devoid of bubbles and in the bubbly flow regime. With decreasing depth and pressure the superficial gas velocity will increase due to volatile exsolution and expansion (**Figure 7**). Although possible in principle, it remains controversial whether the erupting magma transitions to regimes other than bubbly flow (Wilson 1999, Parfitt 2004). However, in the case of appreciable exsolved gas fractions within the storage reservoir, it could be feasible that gas accumulation and bubble coalescence result in flow that is not bubbly (Vergniolle & Jaupart 1986). The magma-gas mixture will exit the vent at speeds of $\sqrt{2gh} \sim 10$–100 m s^{-1} (Wilson 1999), where h is the height to which the magma jets above the surface, typically hundreds of meters in Hawaiian-style eruptions (**Figure 4*b***) (Houghton & Gonnermann 2008).

Rapid decompression of a bubbly Newtonian liquid, analogous to basalt magma, results in inertial stretching and breakup into discrete pieces, if $\mathrm{Re_e} = \rho u_e L/\eta \gtrsim 1$, where $\mathrm{Re_e}$ is the expansion Reynolds number, u_e is the expansion velocity, and L is the height of the expanding liquid volume (Mader et al. 1994, Namiki & Manga 2008). During Hawaiian-style eruptions,

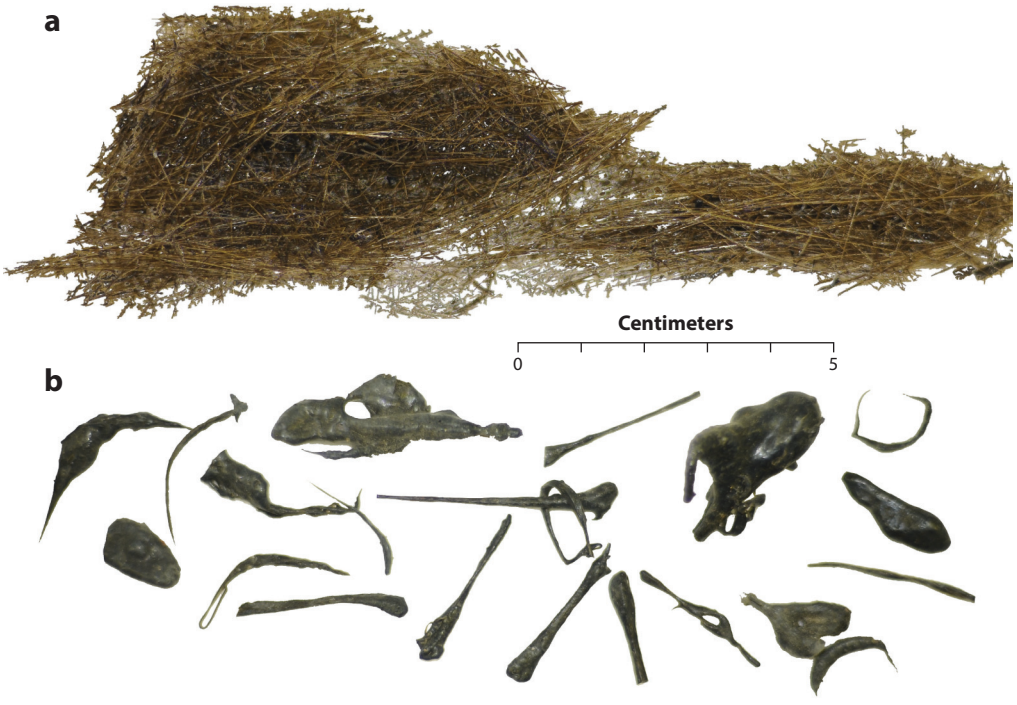

Figure 11

(*a*) Pele's hair and (*b*) Pele's tears from Kilauea volcano, Hawaii. Photographs by Bruce F. Houghton; used with permission.

inertial fragmentation is expected to occur within the uppermost few hundred meters of the conduit and/or above the vent (Mangan & Cashman 1996), where rapid exsolution and expansion of water vapor lead to high magma expansion rates (**Figure 7**). Numerical modeling predicts a difference in velocity between magma and the free gas phase of $\Delta u \sim 100$ m s^{-1} (Wilson 1999), corresponding to $\mathrm{We} = \rho(\Delta u)^2 a/\gamma_s$ and $\mathrm{Re} = \rho a \Delta u/\eta$, where a is the jet radius. Especially above the vent this implies that there should be magma breakup due to interfacial shear between gas and melt (e.g., Lin & Reitz 1998, Eggers & Villermaux 2008), which is corroborated by the abundant presence of Pele's hair during Hawaiian-style eruptions (**Figure 11**) (Villermaux 2012).

5.2.2. Bursting bubbles: Strombolian. Strombolian eruptions are characterized by the bursting of large gas slugs (Gerst et al. 2013), which may form by coalescence of smaller bubbles during ascent or if the conduit geometry is somehow favorable to the accumulation of buoyantly rising bubbles (James et al. 2013). When a slug becomes sufficiently large to break free and rise to the surface, it expands in size as pressure decreases. Near the surface the overlying layer of magma is deformed into a sheet that ruptures, thereby creating a Strombolian explosion through the impulsive releases of gas and the resultant short-lived jet that carries with it pyroclastic fragments of the ruptured magma sheet. Because the magma contains bubbles over a range of sizes (e.g., Lautze & Houghton 2005), the sheet ruptures into a polyhedral network of holes and filaments that are flung outward at high velocities by the rapid expansion and outflow of gas, with inertial forces stretching the filaments until they break up into pyroclasts (**Figure 9**) (Gerst et al. 2013).

6. HYDROMAGMATIC FRAGMENTATION

Hydromagmatic eruptions, also referred to as phreatomagmatic, result from the interaction between magma and external water, either groundwater or surface water (Walker 1973). Water-magma interaction can range from negligibly small water-to-melt ratios to dominantly water controlled (Morrissey et al. 2000, Wohletz et al. 2013). Consequently, both magmatic and hydromagmatic fragmentation may operate simultaneously (Self & Sparks 1978). Hydromagmatic explosions are due to the transfer of heat from melt to water at timescales of microseconds or shorter, resulting in superheating, nucleation of vapor, and, potentially, pressure-induced detonation (Wohletz 1983). Fragmentation itself is in part caused by the stresses associated with a cyclic process of vapor film generation and collapse (Buchanan & Dullforce 1973; Board et al. 1974, 1975; Corradini 1991), and additional fragmentation takes place within the turbulent explosion jet (Mastin 2007).

Fragmentation by water vaporization involves repeated cycles of (*a*) vapor film formation at the melt-water interface; (*b*) vapor film expansion, condensation, and collapse, leading to instabilities that fragment melt at the interface; and (*c*) increased heat transfer as new surface area is created. The fragmentation process at the melt-water interface may involve several mechanisms (Sheridan & Wohletz 1983), including (*a*) water jetting during vapor film collapse; (*b*) stress waves upon impact of the collapsing vapor film; (*c*) hydrodynamic instability of the melt-water interface; and (*d*) thermal stresses within the quenched melt.

Fragmentation intensity and mechanisms depend on the specific melt-water interface area, water-to-melt mass ratio, and magma temperature. The greater the specific melt-water surface area—which depends, among other things, on melt-water intermingling and is affected by viscosity—the more efficient the heat transfer. During fragmentation the melt-water surface area increases rapidly, resulting in a positive feedback between fragmentation and heat transfer (Büttner et al. 2005). The ratio of mechanical energy (i.e., the fragmentation energy of magma and country rock, as well as kinetic energy) to thermal energy prior to fragmentation is called the conversion ratio. It depends on the water-to-melt mass ratio, which strongly affects the degree of fragmentation and the fragment size (**Figure 12**).

Fragmentation by collapse of the superheated vapor film is thought to cause brittle fracture of the melt, thereby producing blocky and platy grains (Wohletz 1983, Heiken & Wohletz 1985, Büttner et al. 1999). Hydrodynamic instabilities of the melt-vapor interface may distort it into a corrugated shape, not only increasing the melt-vapor interface but also enhancing fragmentation into convoluted, drop-like and platy fragments (Wohletz 1983, Heiken & Wohletz 1985). In addition to primary hydromagmatic fragmentation, turbulent energy dissipation within the phreatomagmatic jet may result in secondary fragmentation by liquid breakup as well as brittle fragmentation, if water-to-melt ratios are high. At high water-to-melt ratios the magma will rapidly quench within the jet to form sub-millimeter-thick glassy rinds. Turbulent velocity fluctuations are then expected to cause tensile stresses capable of fragmenting these glassy rinds, perhaps accounting for a significant portion of the fine ash produced during phreatomagmatic eruptions (Mastin 2007, Mastin et al. 2009, Wohletz et al. 1989). However, highly vesicular magma may be less susceptible to such secondary fragmentation (Patel et al. 2013).

7. SHEAR FRAGMENTATION

Cyclic eruption activity and some of the observed seismicity during effusive eruptions of high-viscosity magma are thought to be the consequence of brittle shear failure of the ascending magma (Voight et al. 1999, Harrington & Brodsky 2007, Lavallée et al. 2008, Tuffen et al. 2008, Buurman

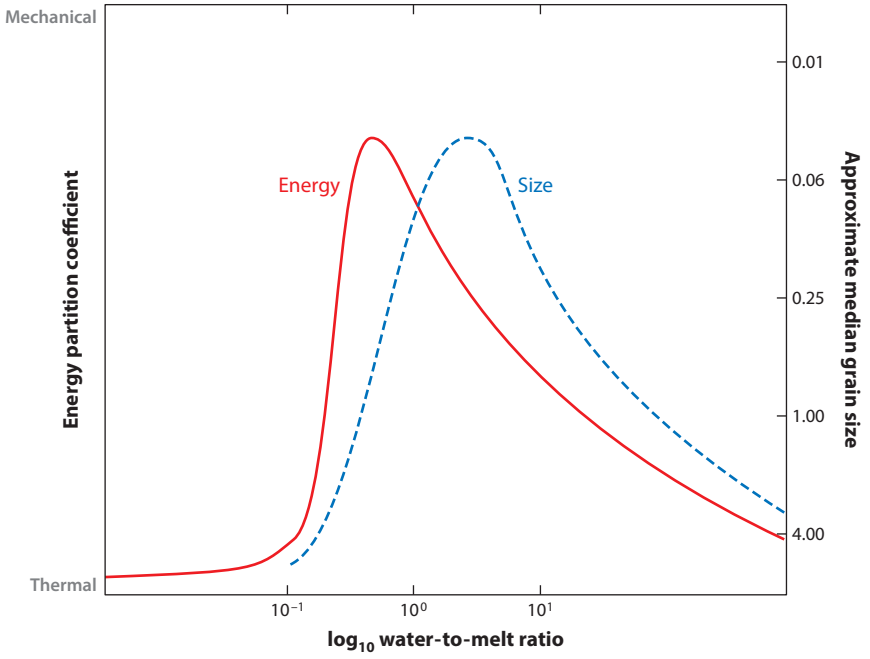

Figure 12

Schematic diagram illustrating the correlation between grain size and the partitioning between thermal and mechanical energy, both as function of the water-to-melt ratio. Figure modified after Wohletz et al. (2013).

& West 2013, Pallister et al. 2013). Such shear fragmentation occurs if strain rates near the conduit walls become sufficiently high to intersect the glass transition (Goto 1999, Gonnermann & Manga 2003, Tuffen et al. 2003). This may produce intermittent permeable pathways to facilitate enhanced outgassing, thereby affecting the explosive potential (Gonnermann & Manga 2003, 2005; Tuffen et al. 2003; Castro et al. 2012), a hypothesis that is consistent with measurements of volatile contents in pyroclastic obsidian (Rust et al. 2004, Cabrera et al. 2011) as well as observations of magma degassing during effusive eruptions (Holland et al. 2011, Castro et al. 2014, Scharff et al. 2014). Shear fragmentation is attained experimentally at stresses of approximately 10–100 MPa, corresponding to strain rates on the order of 10^{-2} to 10^{-4} s^{-1} and is affected by the presence of crystals (e.g., Lavallée et al. 2007, Kennedy et al. 2009, Laumonier et al. 2011, Cordonnier et al. 2012).

8. PRODUCTS OF FRAGMENTATION

8.1. Fragmentation Energy and Fragment Size

Fragmentation converts the potential energy from the compressed gas inside bubbles into the kinetic energy and surface energy of fractures (Alidibirov 1994). Consequently, the size of pyroclasts provides a direct record of the fragmentation process, with small fragment size corresponding to high surface energy consumption during the fragmentation process. Grady (1982) derived an energy balance for a hypothetical isothermal body undergoing a rapid expansion. The instantaneous thermodynamic and kinematic state is determined by the density, ρ, the rate of

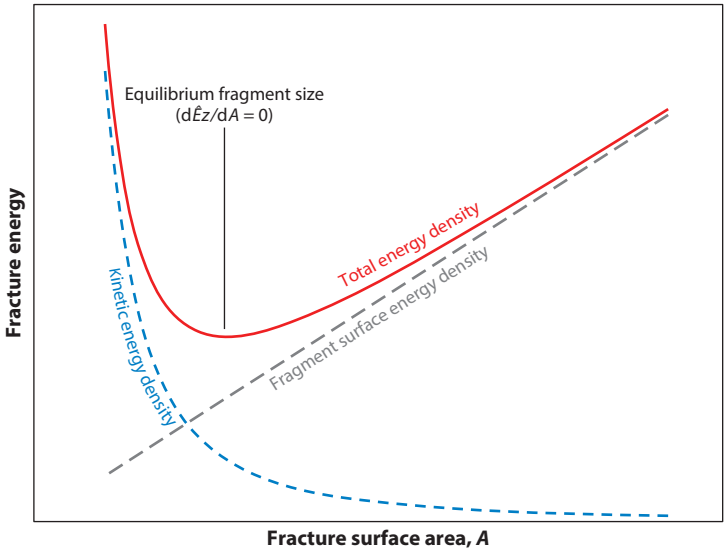

Figure 13

Kinetic energy density, $\hat{E}_k$, and surface energy density, $\hat{E}_s$, which determine the characteristic equilibrium fragment size, d (Grady 1982).

density change, $\dot{\rho}$, and the temperature. It is assumed that expansion causes fragmentation and that the available energy for fragmentation is partially balanced by the new surface energy associated with fragmentation. Because particles will move apart at high velocities after fragmentation, a large portion of the kinetic energy remains in the system. Consequently, the initial energy that caused fragmentation must be converted into some balance of postfragmentation kinetic energy and surface energy. This energy balance can be hypothesized to represent an equilibrium fragment size for a given initial expansion rate $\dot{\rho}$ (**Figure 13**).

In detail, the energy balance for an idealized fragment represented by a spherical mass element of radius $r = b$ can be derived by assuming that it is expanding uniformly from its center at a rate $\dot{r} = -\dot{\rho}r/3\rho$. The kinetic energy, E_k, about the center of mass of this element is obtained by integrating the kinetic energy of a spherical shell, $2\pi\rho\dot{r}^2r^2\mathrm{d}r$, from $r = 0$ to $r = b$, which gives $E_k = 2\pi\dot{\rho}^2b^5/45\rho$. The resultant kinetic energy density is $\hat{E}_k = 3\dot{\rho}^2/10\rho A^2$ and the surface energy density is $\hat{E}_s = \gamma_e A$, where γ_e is surface energy and $A = 3/b$ is the surface area–to–volume ratio. The total energy density therefore is

$$\hat{E}(A) = \frac{3\dot{\rho}^2}{10\rho A^2} + \gamma_e A. \tag{3}$$

$\hat{E}$ is equal to the prefragmentation kinetic energy, and for brittle magma fragmentation it is conceptually equivalent to the potential energy of the compressed gas inside bubbles (Alidibirov 1994, Alatorre-Ibargüengoitia et al. 2010). The equilibrium fragment size is determined by the condition $\mathrm{d}\hat{E}/\mathrm{d}A = 0$ (**Figure 13**) and gives

$$A_{\mathrm{equil}} = \left(\frac{3\dot{\rho}^2}{5\rho\gamma_e}\right)^{1/3}. \tag{4}$$

Yew & Taylor (1994) extended this energy balance using a thermodynamic theory and predicted a similar characteristic fragment size.

The above treatment is applicable to expanding magma undergoing fluid-dynamic breakup or brittle fragmentation. For the latter, the equilibrium fragment size can be expressed in terms of a linear strain rate, $\dot{\varepsilon} = \dot{\rho}/3\rho$, and the material's fracture toughness, $K_c \approx \sqrt{\gamma_e E}$, as

$$d = \left(\frac{\sqrt{20} K_c}{\rho c \dot{\varepsilon}} \right)^{2/3}. \quad (5)$$

Here $c = \sqrt{\mu/\rho}$ is the sound speed, E is Young's modulus, μ is the bulk modulus, and values of K_c for volcanic glasses are $\sim 10^6$ N m$^{-3/2}$ (Gerth & Schnapp 1996, Alatorre-Ibargüengoitia et al. 2010, Kolzenburg et al. 2013).

8.2. Observed Fragment Size Distributions

Although the energy-based theory has been reasonably successful in predicting characteristic fragment sizes, the prediction of size distributions remains an active area of research (e.g., Büttner et al. 2006, Kueppers et al. 2006b, Grady 2010)—in particular, the study of power-law size distributions, typical for pyroclastic deposits (Turcotte 1986, Kaminski & Jaupart 1998, Girault et al. 2014) and also observed in fragmentation experiments (Kueppers et al. 2006a). Because fragmentation by throughgoing fractures is not sufficient to dissipate the strain energy that drives fragmentation, a cascade of fractures with successively smaller length scales has been suggested. In this model the characteristic length scales obtained from energy balance serve as a functional limit for the fragment size distribution (Grady 2010).

Energy balance dissipation of strain energy may also be broadly consistent with the suggestion that magma permeability affects the size distribution of pyroclastic deposits, because it dissipates gas pressure within centimeter- to decimeter-sized clasts without the need for fragmentation down to the size of individual bubbles (Klug & Cashman 1996, Rust & Cashman 2011). As a corollary, silicic magma should fragment down to a fragment size at which permeable gas escape is rapid, causing the magma flow within the conduit to effectively transition to a low-viscosity gas-pyroclast mixture of significantly lower frictional pressure loss, thereby significantly affecting eruption dynamics (Papale 2001, Girault et al. 2014).

Whereas pressure diffusion by permeable gas flow may set an upper length scale for fragment size, the smallest grains in pyroclastic deposits tend to be bubble-wall shards (Sparks & Wilson 1976, Heiken & Wohletz 1985, Rust & Cashman 2011). Accordingly, many deposits have pyroclasts ranging from micrometer-sized ash to decimeter-sized bombs, with a power-law size distribution and exponents of approximately 3–4 (e.g., Kaminski & Jaupart 1998, Girault et al. 2014). Although grain size distributions seem clearly distinguishable between some eruption types (Rust & Cashman 2011 and references therein), the diversity in fragmentation phenomena and magma properties makes it challenging to universally relate grain size distributions to an energy balance.

8.3. Secondary Fragmentation

Pyroclasts formed by magma fragmentation may be reduced to smaller size by secondary fragmentation, due to high-energy collisions within the volcanic conduit. During secondary fragmentation larger clasts are more likely to be fragmented to smaller size than are smaller clasts. Because the number of disruptive collisions scales with the fragmentation depth, the presence of abundant large clasts in pyroclastic deposits may therefore reflect shallow fragmentation. In contrast, large fragmentation depths are expected to result in enhanced ash production, shifting the grain size

distribution of pyroclastic deposits toward larger power-law exponents, all else being equal (Kaminski & Jaupart 1998, Dufek et al. 2012). It should be noted that secondary fragmentation may also occur above the vent within the volcanic jet, and within pyroclastic flows (Kaminski & Jaupart 1998, Wohletz et al. 1989). Because the clasts produced by secondary fragmentation are angular in shape, they may be indistinguishable from those produced by primary fragmentation. In contrast, low-energy collisions will result in rounding of clasts but will also produce ash (Manga et al. 2011).

9. PERSPECTIVES AND FUTURE DIRECTIONS

Magma fragmentation is of crucial importance for volcanic eruptions. It fundamentally affects the state and the dynamics of how magma is transported to, at, and above the planet's surface. Of particular consequence is how fragmentation affects the manner and intensity by which magmatic gases are released and potential energy is transformed into surface energy and kinetic energy. This energy transformation determines the ensuing number and size of volcanic fragments, in particular volcanic ash, as well as their transport into and ultimately within the planet's atmosphere. The implications can be of global consequence, with potentially profound societal and health impacts (Horwell & Baxter 2006, Self 2006, Guffanti et al. 2008, Martin et al. 2009, Langmann et al. 2012, Wilson et al. 2012), as well as significant climate effects (Robock 2000, Mann 2007, Santer et al. 2014).

Magma fragmentation is complex, not only because of the viscoelastic nature of silicate melt, but also because of the presence of a gas phase, which makes the magma a structurally complex mixture. A case in point is the critical fragmentation stress predicted from fiber elongation experiments versus the tensile strength determined from decompression experiments on vesicular samples, which is about 2 orders of magnitude smaller.

Similarly, the potential relationship between bubble nucleation and brittle magma fragmentation remains to be fully understood (Toramaru 2006). Large decompression rates are required for both bubble nucleation (Toramaru 1995, 2006) and fragmentation, but are sustainable only over short distances and should be associated with high magma viscosity. The latter requires low concentrations of dissolved water and is contingent on the formation and presence of bubbles, as is fragmentation itself. In contrast, high bubble nucleation rates require that the magma is supersaturated with dissolved water. These conditions are rather restrictive in terms of a potential interdependency between bubble nucleation and magma fragmentation (Gonnermann & Houghton 2012).

Another complexity arises from the nature and occurrence of concomitant solid and liquid fragmentation, a subject already alluded to by Villermaux (2007). It is augmented by the possibility of strain localization, due to the deformation of bubbles (Wright & Weinberg 2009, Okumura et al. 2010), and by the frequent presence of crystals, sometimes at very high concentrations (e.g., Sable et al. 2006, 2009; Giachetti et al. 2010; Cordonnier et al. 2012). Magma fragmentation therefore transcends continuum mechanics and the conventional boundaries between fluid and solid mechanics, and it thus offers a wide range of opportunities for future research.

Fragmentation likely plays a role on a number of planetary bodies, where it may not necessarily be restricted to silicate melts. Earth's moon bears ample evidence for explosive eruptions of basaltic magma (e.g., Rutherford & Papale 2009), whereas the *Galileo* spacecraft observed large eruption plumes above Jupiter's moon Io, containing ash composed of silicates and sulfurous compounds (Geissler & McMillan 2008). Perhaps a more exotic example is the eruption plumes emanating from Saturn's icy moon Enceladus, which are thought to be composed of gas and ice (Spencer & Nimmo 2013), although the presence of particulates is likely due to condensation and freezing of water vapor.

SUMMARY POINTS

1. The glass transition is a reversible transition between elastic/brittle and viscous/ductile behavior in amorphous materials. It is related to the relaxation rate of the molecular structure, which is inversely proportional to the Maxwell time, defined as the ratio of viscosity to elastic modulus. If deformation rates are much larger than the reciprocal Maxwell time, the material will respond in an elastic or brittle manner; otherwise, it will respond viscously. Brittle failure is a consequence of the breaking of bridging oxygen bonds within the molecular silica network. Because viscosity is strongly temperature dependent, the glass transition is a function of both temperature and deformation rate.
2. Brittle fragmentation requires magma of high viscosity. High viscosity resists bubble growth and leads to bubble overpressure. High viscosity also results in steep pressure gradients, due to viscous stresses during magma flow within the conduit. Furthermore, brittle deformation requires that deformation rates exceed the structural relaxation rate, which scales with reciprocal viscosity.
3. Fragmentation of mafic magma is by fluid-dynamic breakup, due to inertial forces generated during the expansion of magmatic gases and turbulence within the gas-magma jet.
4. External water may play a role during most explosive eruptions. At large water-to-melt ratios, fragmentation is a result of heat transfer across the melt-water interface. This results in partial quenching of the melt, as well as dynamic stresses due to vaporization and cooling, leading to brittle fragmentation.
5. Brittle fragmentation by shear near the conduit walls is seismically detectable, provides pathways for gas escape, and affects the dynamic conditions for effusive or explosive activity.
6. Pyroclastic fragment sizes depend on the energy balance of converting the potential energy of compressed magmatic gases into new surface area and kinetic energy. Collisions between magma fragments result in secondary fragmentation, which shifts fragment size distributions toward smaller fragment size and larger power-law exponents.

DISCLOSURE STATEMENT

The author is not aware of any affiliations, memberships, funding, or financial holdings that might be perceived as affecting the objectivity of this review.

ACKNOWLEDGMENTS

Endeavoring to chronicle the complex and diverse phenomena of magma fragmentation has been a challenging undertaking. A large body of published work has contributed to my understanding of this subject. Only the most relevant publications could be cited, and I apologize for any unintended omissions. This work has in part been supported by the National Science Foundation under grants EAR-1145187, EAR-1250451, and EAR-1348072. Any opinions, findings, and conclusions, or recommendations expressed in this material are those of the author and do not necessarily reflect the views of the National Science Foundation.

LITERATURE CITED

Alatorre-Ibargüengoitia MA, Scheu B, Dingwell DB, Delgado-Granados H, Taddeucci J. 2010. Energy consumption by magmatic fragmentation and pyroclast ejection during Vulcanian eruptions. *Earth Planet. Sci. Lett.* 291:60–69

Alidibirov M. 1994. A model for viscous magma fragmentation during volcanic blasts. *Bull. Volcanol.* 56:459–65

Alidibirov M, Dingwell DB. 1996. Magma fragmentation by rapid decompression. *Nature* 380:146–48

Batchelor GK. 1967. *An Introduction to Fluid Dynamics*. Cambridge, UK: Cambridge Univ. Press

Blower JD. 2001. Factors controlling permeability-porosity relationships in magma. *Bull. Volcanol.* 63:497–501

Board SJ, Farner CL, Poole DH. 1974. Fragmentation in thermal explosions. *Int. J. Heat Mass Transfer.* 17:331–39

Board SJ, Hall RW, Hall RS. 1975. Detonation of fuel coolant explosions. *Nature* 254:319–21

Branca S, Del Carlo P. 2005. Types of eruptions of Etna volcano AD 1670–2003: implications for short-term eruptive behavior. *Bull. Volcanol.* 67:732–42

Buchanan DJ, Dullforce TA. 1973. Mechanism for vapour explosions. *Nature* 245:32–34

Büttner R, Dellino P, Raue H, Sonder I, Zimanowski B. 2006. Stress-induced brittle fragmentation of magmatic melts: theory and experiments. *J. Geophys. Res.* 111:B08204

Büttner R, Dellino P, Zimanowski B. 1999. Identifying magma-water interaction from the surface features of ash particles. *Nature* 401:688–90

Büttner R, Zimanowski B, Mohrholz CO. 2005. Analysis of thermohydraulic explosion energetics. *J. Appl. Phys.* 98:043524

Buurman H, West ME. 2013. Magma fracture and hybrid earthquakes in the conduit of Augustine Volcano. *Geophys. Res. Lett.* 40:6038–42

Cabrera A, Weinberg RF, Wright HMN, Zlotnik S, Cas RAF. 2011. Melt fracturing and healing: a mechanism for degassing and origin of silicic obsidian. *Geology* 39:67–70

Castro JM, Bindeman IN, Tuffen H, Schipper I. 2014. Explosive origin of silicic lava: textural and δD–H_2O evidence for pyroclastic degassing during rhyolite effusion. *Earth Planet. Sci. Lett.* 405:52–61

Castro JM, Cordonnier B, Tuffen H, Tobin MJ, Puskar L, et al. 2012. The role of melt-fracture degassing in defusing explosive rhyolite eruptions at volcán Chaitén. *Earth Planet. Sci. Lett.* 333–34:63–69

Clarke AB. 2013. Unsteady explosive activity: Vulcanian eruptions. See Fagents et al. 2013, pp. 129–52

Cordonnier B, Caricchi L, Pistone M, Castro J, Hess KU, et al. 2012. The viscous-brittle transition of crystal-bearing silicic melt: direct observation of magma rupture and healing. *Geology* 40:611–14

Corradini ML. 1991. Vapor explosions: a review of experiments for accident analysis. *Nucl. Saf.* 32:337–62

Dingwell DB. 1996. Volcanic dilemma: flow or blow? *Science* 273:1054–55

Dingwell DB. 1997. The brittle-ductile transition in high-level granitic magmas: material constraints. *J. Petrol.* 38:1635–44

Dingwell DB, Webb SL. 1989. Structural relaxation in silicate melts and non-Newtonian melt rheology in geological processes. *Phys. Chem. Mater.* 16:508–16

Dobran F. 1992. Nonequilibrium flow in volcanic conduits and application to the eruptions of Mt. St. Helens on May 19, 1980, and Vesuvius in AD 79. *J. Volcanol. Geotherm. Res.* 49:285–311

Dombrowski N, Fraser RP. 1954. A photographic investigation into the disintegration of liquid sheets. *Philos. Trans. R. Soc. A* 247:101–30

Dufek J, Bergantz GW. 2005. Transient two-dimensional dynamics in the upper conduit of a rhyolitic eruption: a comparison of closure models for granular stress. *J. Volcanol. Geotherm. Res.* 143:113–32

Dufek J, Manga M, Patel A. 2012. Granular disruption during explosive volcanic eruptions. *Nat. Geosci.* 5:561–64

Eggers J. 1993. Universal pinching of 3D axisymmetric free-surface flow. *Phys. Rev. Lett.* 71:3458–60

Eggers J, Villermaux E. 2008. Physics of liquid jets. *Rep. Prog. Phys.* 71:036601

Fagents SA, Gregg TKP, Lopes RMC, eds. 2013. *Modeling Volcanic Processes: The Physics and Mathematics of Volcanism*. New York: Cambridge Univ. Press

Eichelberger JC. 1995. Silicic volcanism. *Annu. Rev. Earth Planet. Sci.* 23:41–63

Eichelberger JC, Carrigan CR, Westrich HR, Price RH. 1986. Non-explosive silicic volcanism. *Nature* 323:598–602

Geissler PE, McMillan MT. 2008. Galileo observations of volcanic plumes on Io. *Icarus* 197:505–18

Gerst A, Hort M, Aster RC, Johnson JB, Kyle PR. 2013. The first second of volcanic eruptions from the Erebus volcano lava lake, Antarctica—energies, pressures, seismology, and infrasound. *J. Geophys. Res. Solid Earth* 118:3318–40

Gerth U, Schnapp JD. 1996. Investigation of mechanical properties of natural glasses using indentation methods. *Chem. Erde* 56:398–403

Giachetti T, Druitt TH, Burgisser A, Arbaret L, Galven C. 2010. Bubble nucleation, growth and coalescence during the 1997 Vulcanian explosions of Soufrière Hills Volcano, Montserrat. *J. Volcanol. Geotherm. Res.* 193:215–31

Giordano D, Dingwell DB. 2003a. The kinetic fragility of natural silicate melts. *J. Phys. Condens. Matter* 15:S945–54

Giordano D, Dingwell DB. 2003b. Viscosity of hydrous Etna basalt: implications for Plinian-style basaltic eruptions. *Bull. Volcanol.* 65:8–14

Girault F, Carazzo G, Tait S, Ferrucci F, Kaminski É. 2014. The effect of total grain-size distribution on the dynamics of turbulent volcanic plumes. *Earth Planet. Sci. Lett.* 394:124–34

Goepfert K, Gardner JE. 2010. Influence of pre-eruptive storage conditions and volatile contents on explosive Plinian style eruptions of basic magma. *Bull. Volcanol.* 72:511–21

Gonnermann HM, Houghton BF. 2012. Magma degassing during the Plinian eruption of Novarupta, Alaska, 1912. *Geochem. Geophys. Geosyst.* 13:Q10009

Gonnermann HM, Manga M. 2003. Explosive volcanism may not be an inevitable consequence of magma fragmentation. *Nature* 426:432–35

Gonnermann HM, Manga M. 2005. Flow banding in obsidian: a record of evolving textural heterogeneity during magma fragmentation. *Earth Planet. Sci. Lett.* 236:135–47

Gonnermann HM, Manga M. 2007. The fluid mechanics inside a volcano. *Annu. Rev. Fluid Mech.* 39:321–56

Goto A. 1999. A new model for volcanic earthquake at Unzen Volcano: melt rupture model. *Geophys. Res. Lett.* 26:2541–44

Grady DE. 1982. Local inertial effects in dynamic fragmentation. *J. Appl. Phys.* 53:322–25

Grady DE. 2010. Length scales and size distributions in dynamic fragmentation. *Int. J. Fract.* 163:85–99

Guffanti M, Mayberry GC, Casadevall TJ, Wunerman R. 2008. Volcanic hazards to airports. *Nat. Hazards.* doi: 10.1007/s11069-008-9254-2

Harrington RM, Brodsky EE. 2007. Volcanic hybrid earthquakes that are brittle-failure events. *Geophys. Res. Lett.* 34:L06308

Heiken G, Wohletz K. 1985. *Volcanic Ash*. Berkeley/Los Angeles: Univ. Calif. Press

Holland ASP, Watson IM, Phillips JC, Caricchi L, Dalton MP. 2011. Degassing processes during lava dome growth: insights from Santiaguito lava dome, Guatemala. *J. Volcanol. Geotherm. Res.* 202:153–66

Horwell CJ, Baxter PJ. 2006. The respiratory health hazards of volcanic ash: a review for volcanic risk mitigation. *Bull. Volcanol.* 69:1–24

Houghton BF, Gonnermann HM. 2008. Basaltic explosive volcanism: constraints from deposits and models. *Chem. Erde* 68:117–40

Houghton BF, Rymer H, Stix J, McNutt S, Sigurdsson H, eds. 2000a. *Encyclopedia of Volcanoes*. San Diego, CA: Academic

Houghton BF, Wilson CJN, Smith RT, Gilbert JS. 2000b. Phreatoplinian eruptions. See Houghton et al. 2000a, pp. 513–25

Hui HJ, Zhang YX. 2007. Toward a general viscosity equation for natural anhydrous and hydrous silicate melts. *Geochim. Cosmochim. Acta* 71:403–16

Huisman FM, Friedman SR, Taborek P. 2012. Pinch-off dynamics in foams, emulsions and suspensions. *Soft Matter* 8:6767–74

Ichihara M, Rittel D, Sturtevant B. 2002. Fragmentation of a porous viscoelastic material: implications to magma fragmentation. *J. Geophys. Res.* 107(B10):2229

Israelachvili JN. 2011. *Intermolecular and Surface Forces.* San Diego, CA: Academic. 3rd ed.

James MR, Lane SJ, Houghton BF. 2013. Unsteady explosive activity: Strombolian eruptions. See Fagents et al. 2013, pp. 107–29

Jellinek AM, DePaolo DJ. 2003. A model for the origin of large silicic magma chambers: precursors of caldera-forming eruptions. *Bull. Volcanol.* 65:363–81
Kaminski É, Jaupart C. 1998. The size distribution of pyroclasts and the fragmentation sequence in explosive volcanic eruptions. *J. Geophys. Res.* 103(B12):29759–79
Kennedy LA, Russell JK, Nelles E. 2009. Origins of Mount St. Helens cataclasites: experimental insights. *Am. Mineral.* 94:995–1004
Kerrick E, Jacobs GK. 1981. A modified Redlich-Kwong equation for H_2O, CO_2, and H_2O-CO_2 mixtures at elevated pressures and temperatures. *Am. J. Sci.* 281:735–67
Klug C, Cashman KV. 1996. Permeability development in vesiculating magmas: implications for fragmentation. *Bull. Volcanol.* 58:87–100
Kolzenburg S, Russell JK, Kennedy LA. 2013. Energetics of glass fragmentation: experiments on synthetic and natural glasses. *Geochem. Geophys. Geosyst.* 14:4936–51
Koyaguchi T. 2005. An analytical study for 1-dimensional steady flow in volcanic conduits. *J. Volcanol. Geotherm. Res.* 143:29–52
Koyaguchi T, Mitani NK. 2005. A theoretical model for fragmentation of viscous bubbly magmas in shock tubes. *J. Geophys. Res.* 110:B10202
Koyaguchi T, Scheu B, Mitani NK, Melnik O. 2008. A fragmentation criterion for highly viscous bubble magmas estimated from shock tube experiments. *J. Volcanol. Geotherm. Res.* 178:58–71
Kowalewski TA. 1996. On the separation of droplets from a liquid jet. *Fluid Dyn. Res.* 17:121–45
Kueppers U, Perugini D, Dingwell DB. 2006a. "Explosive energy" during volcanic eruptions from fractal analysis of pyroclasts. *Earth Planet. Sci. Lett.* 248:800–7
Kueppers U, Scheu B, Spieler O, Dingwell DB. 2006b. Fragmentation efficiency of explosive volcanic eruptions: a study of experimentally generated pyroclasts. *J. Volcanol. Geotherm. Res.* 153:125–35
Langmann B, Folch A, Hensch M, Matthias V. 2012. Volcanic ash over Europe during the eruption of Eyjafjallajökull on Iceland, April–May 2010. *Atmos. Environ.* 48:1–8
Laumonier M, Arbaret L, Burgisser A, Champallier R. 2011. Porosity redistribution enhanced by strain localization in crystal-rich magmas. *Geology* 39:715–18
Lautze NC, Houghton BF. 2005. Physical mingling of magma and complex eruption dynamics in the shallow conduit at Stromboli volcano, Italy. *Geology* 33:425–28
Lavallée Y, Hess KU, Cordonier B, Dingwell DB. 2007. Non-Newtonian rheological law for highly crystalline dome lavas. *Geology* 35:843–46
Lavallée Y, Meredith PG, Dingwell DB, Hess KU, Wassermann J, et al. 2008. Seismogenic lavas and explosive eruption forecasting. *Nature* 453:507–10
Lensky NG, Lyakhovsky V, Navon O. 2001. Radial variations of melt viscosity around growing bubbles and gas overpressure in vesiculating magmas. *Earth Planet. Sci. Lett.* 186:1–6
Lin SP, Reitz RD. 1998. Drop and spray formation from a liquid jet. *Annu. Rev. Fluid Mech.* 30:85–105
Liu Y, Zhang YX, Behrens H. 2005. Solubility of H_2O in rhyolitic melts at low pressures and a new empirical model for mixed H_2O-CO_2 solubility in rhyolitic melts. *J. Volcanol. Geotherm. Res.* 143:219–35
Mader HM. 1998. Conduit flow and fragmentation. *Geol. Soc. Lond. Spec. Publ.* 145:51–71
Mader HM, Llewellin EW, Mueller SP. 2013. The rheology of two-phase magmas: a review and analysis. *J. Volcanol. Geotherm. Res.* 257:135–58
Mader HM, Zhang Y, Phillips JC, Sparks RSJ, Sturtevant B, Stolper E. 1994. Experimental simulations of explosive degassing of magma. *Nature* 372:85–88
Manga M, Patel A, Dufek J. 2011. Rounding of pumice clasts during transport: field measurements and laboratory studies. *Bull. Volcanol.* 73:321–33
Mangan MT, Cashman KV. 1996. The structure of basaltic scoria and reticulite and inferences for vesiculation, foam formation, and fragmentation in lava fountains. *J. Volcanol. Geotherm. Res.* 73:1–18
Mann ME. 2007. Climate over the past two millennia. *Annu. Rev. Earth Planet. Sci.* 35:111–36
Martel C, Dingwell DB, Spieler O, Pichavant M, Wilke M. 2000. Fragmentation of foamed silicic melts: an experimental study. *Earth Planet. Sci. Lett.* 178:47–58
Martel C, Dingwell DB, Spieler O, Pichavant M, Wilke M. 2001. Experimental fragmentation of crystal- and vesicle-bearing silicic melts. *Bull. Volcanol.* 63:398–405

Martin RS, Watt SFL, Pyle DM, Mather TA, Matthews NE, et al. 2009. Environmental effects of ashfall in Argentina from the 2008 Chaitén volcanic eruption. *J. Volcanol. Geotherm. Res.* 184:462–72

Mastin LG. 2002. Insights into volcanic conduit flow from an open-source numerical model. *Geochem. Geophys. Geosyst.* 3. doi: 10.1029/2001GC000192

Mastin LG. 2005. The controlling effect of viscous dissipation on magma flow in silicic conduits. *J. Volcanol. Geotherm. Res.* 143:17–28

Mastin LG. 2007. Generation of fine hydromagmatic ash by growth and disintegration of glassy rinds. *J. Geophys. Res.* 112:B02203

Mastin LG, Spieler O, Downey WS. 2009. An experimental study of hydromagmatic fragmentation through energetic, non-explosive magma-water mixing. *J. Volcanol. Geotherm. Res.* 180:161–70

Miskin MZ, Jaeger HM. 2012. Droplet formation and scaling in dense suspensions. *PNAS* 109:4389–94

Moitra P, Gonnermann HM, Houghton BF. 2010. *Rheological effects of microlites on the Plinian eruption of basaltic magma*. Presented at AGU Fall Meet., Dec. 13–17, San Francisco. Abstr. V43B-2371

Morrissey M, Zimanowski B, Wohletz K, Bütter R. 2000. Phreatomagmatic fragmentation. See Houghton et al. 2000a, pp. 430–45

Moynihan CT. 1995. Structural relaxation and the glass transition. *Rev. Mineral. Geochem.* 32:1–19

Mueller S, Scheu B, Spieler O, Dingwell DB. 2008. Permeability control on magma fragmentation. *Geology* 36:399–402

Mungall JE, Bagdassarov S, Romano C, Dingwell DB. 1996. Numerical modelling of stress generation and microfracturing of vesicle walls in glassy rocks. *J. Volcanol. Geotherm. Res.* 73:33–46

Namiki A, Manga M. 2005. Response of a bubble bearing viscoelastic fluid to rapid decompression: implications for explosive volcanic eruptions. *Earth Planet. Sci. Lett.* 236:269–84

Namiki A, Manga M. 2008. Transition between fragmentation and permeable outgassing of low viscosity magmas. *J. Volcanol. Geotherm. Res.* 169:48–60

Nguyen CT, Gonnermann HM, Houghton BF. 2014. Explosive to effusive transition during the largest volcanic eruption of the 20th century (Novarupta 1912, Alaska). *Geology* 42:703–6

Okumura S, Nakamura M, Nakano T, Uesugi K, Tsuchiyama A. 2010. Shear deformation experiments on vesicular rhyolite: implications for brittle fracturing, degassing, and compaction of magmas in volcanic conduits. *J. Geophys. Res.* 115:B06201

Pallister JS, Cashman KV, Hagstrum JT, Beeler NM, Moran SC, Denlinger RP. 2013. Faulting within the Mount St. Helens conduit and implications for volcanic earthquakes. *Geol. Soc. Am. Bull.* 125:359–76

Papale P. 1999. Strain-induced magma fragmentation in explosive eruptions. *Nature* 397:425–28

Papale P. 2001. Dynamics of magma flow in volcanic conduits with variable fragmentation efficiency and nonequilibrium pumice degassing. *J. Geophys. Res.* 106(B6):11043–65

Parfitt EA. 2004. A discussion of the mechanisms of explosive basaltic eruptions. *J. Volcanol. Geotherm. Res.* 134:77–107

Patel A, Manga M, Carey RJ, Degruyter W. 2013. Effects of thermal quenching on mechanical properties of pyroclasts. *J. Volcanol. Geotherm. Res.* 258:24–30

Proussevitch AA, Sahagian DL, Anderson AT. 1993. Dynamics of diffusive bubble growth in magmas: isothermal case. *J. Geophys. Res.* 98(B12):22283–307

Robock A. 2000. Volcanic eruptions and climate. *Rev. Geophys.* 38:191–219

Romano C, Mungall JE, Sharp T, Dingwell DB. 1996. Tensile strengths of hydrous vesicular glasses: an experimental study. *Am. Mineral.* 81:1148–54

Rust AC, Cashman KV. 2004. Permeability of vesicular silicic magma: inertial and hysteresis effects. *Earth Planet. Sci. Lett.* 228:93–107

Rust AC, Cashman KV. 2011. Permeability controls on expansion and size distributions of pyroclasts. *J. Geophys. Res.* 116:B11202

Rust AC, Cashman KV, Wallace PJ. 2004. Magma degassing buffered by vapor flow through brecciated conduit margins. *Geology* 32:349–52

Rutherford MJ, Papale P. 2009. Origin of basalt fire-fountain eruptions on Earth versus the Moon. *Geology* 37:219–22

Sable JE, Houghton BF, Del Carlo P, Coltelli M. 2006. Changing conditions of magma ascent and fragmentation during the Etna 122 BC basaltic Plinian eruption: evidence from clast microtextures. *J. Volcanol. Geotherm. Res.* 158:333–54

Sable JE, Houghton BF, Wilson CJN, Carey RJ. 2009. Eruption mechanisms during the climax of the Tarawera 1886 basaltic Plinian eruption inferred from microtextural characteristics of the deposits. *Spec. Publ. IAVCEI* 2:129–54

Santer BD, Bonfils C, Painter JF, Zelinka MD, Mears C, et al. 2014. Volcanic contribution to decadal changes in tropospheric temperature. *Nat. Geosci.* 7:185–89

Scharff L, Hort M, Gerst A. 2014. The dynamics of the dome at Santiaguito volcano, Guatemala. *Geophys. J. Int.* 197:926–42

Scheu B, Spieler O, Dingwell DB. 2006. Dynamics of explosive volcanism at Unzen volcano: an experimental contribution. *Bull. Volcanol.* 69:175–87

Schipper CI, Castro JM, Tuffen H, James MR, How P. 2013. Shallow vent architecture during hybrid explosive-effusive activity at Cordón Caulle (Chile, 2011–12): evidence from direct observations and pyroclast textures. *J. Volcanol. Geotherm. Res.* 262:25–37

Schlegel JP, Sharma S, Cuenca RM, Hibiki T, Ishii M. 2014. Local flow structure beyond bubbly flow in large diameter channels. *Int. J. Heat Fluid Flow* 47:42–52

Self S. 2006. The effects and consequences of very large explosive volcanic eruptions. *Philos. Trans. R. Soc. A* 364:2073–97

Self S, Sparks RSJ. 1978. Characteristics of widespread pyroclastic deposits formed by the interaction of silicic magma and water. *Bull. Volcanol.* 41:196–212

Sheridan MF, Wohletz KH. 1983. Hydrovolcanism: basic consideration and review. *J. Volcanol. Geotherm. Res.* 17:1–29

Shikhmurzaev YD. 2000. Coalescence and capillary breakup of liquid volumes. *Phys. Fluids* 12:2386–96

Smith MI, Besseling R, Cates ME, Bertola V. 2010. Dilatancy in the flow and fracture of stretched colloidal suspensions. *Nat. Commun.* 1:114

Sparks RSJ. 1978. The dynamics of bubble formation and growth in magmas: a review and analysis. *J. Volcanol. Geotherm. Res.* 3:1–37

Sparks RSJ, Wilson L. 1976. A model for the formation of ignimbrite by gravitational column collapse. *J. Geol. Soc. Lond.* 132:441–51

Spencer JR, Nimmo F. 2013. Enceladus: an active ice world in the Saturn system. *Annu. Rev. Earth Planet. Sci.* 41:693–717

Spieler O, Kennedy B, Kueppers U, Dingwell DB, Scheu B, Taddeucci J. 2004. The fragmentation threshold of pyroclastic rocks. *Earth Planet. Sci. Lett.* 226:139–48

Toramaru A. 1995. Numerical study of nucleation and growth of bubbles in viscous magma. *J. Geophys. Res.* 100(B2):1913–31

Toramaru A. 2006. BND (bubble number density) decompression rate meter for explosive volcanic eruptions. *J. Volcanol. Geotherm. Res.* 154:303–16

Tuffen H, Dingwell DB, Pinkerton H. 2003. Repeated fracture and healing of silicic magma generate flow banding and earthquakes? *Geology* 31:1089–92

Tuffen H, Smith R, Sammonds PR. 2008. Evidence for seismogenic fracture of silicic magma *Nature* 453:511–14

Turcotte DL. 1986. Fractals and fragmentation. *J. Geophys. Res.* 91(B2):1921–26

Vergniolle S, Jaupart C. 1986. Separated two-phase flow and basaltic eruptions. *J. Geophys. Res.* 91:12842–60

Villermaux E. 2007. Fragmentation. *Annu. Rev. Fluid Mech.* 39:419–46

Villermaux E. 2012. The formation of filamentary structures from molten silicates: Pele's hair, angel hair, and blown clinker. *C. R. Méc.* 340:555–64

Voight B, Sparks RSJ, Miller AD, Stewart RC, Hoblitt RP, et al. 1999. Magma flow instability and cyclic activity at Soufriere Hills volcano, Montserrat, British West Indies. *Science* 283:1138–42

Walker GP. 1973. Explosive volcanic eruptions—a new classification scheme. *Geol. Rundsch.* 62:431–46

Webb SL, Dingwell DB. 1990a. Non-Newtonian rheology of igneous melts at high stresses and strain rates: experimental results for rhyolite, andesite, basalt and nephelinite. *J. Geophys. Res.* 95(B10):15695–701

Webb SL, Dingwell DB. 1990b. The onset of non-Newtonian rheology of silicate melts: a fiber elongation study. *Phys. Chem. Miner.* 17:125–32

White JDL, Houghton BF. 2000. Surtseyan and related phreatomagmatic eruptions See Houghton et al. 2000a, pp. 495–511

Wilson L. 1999. Explosive volcanic eruptions. X. The influence of pyroclast size distributions and released magma gas content on the eruption velocities of pyroclasts and gas in Hawaiian and Plinian eruptions. *Geophys. J. Int.* 136:609–19

Wilson L, Sparks RSJ, Walker GPL. 1980. Explosive volcanic eruptions. IV. The control of magma properties and conduit geometry on eruption column behaviour. *Geophys. J. R. Astron. Soc.* 63:117–48

Wilson TM, Stewart C, Sword-Daniels V, Leonard GS, Johnston DM, et al. 2012. Volcanic ash impacts on critical infrastructure. *Phys. Chem. Earth* 45–46:5–23

Wohletz KH. 1983. Mechanisms of hydrovolcanic pyroclast formation: grain-size, scanning electron microscopy, and experimental studies. *J. Volcanol. Geotherm. Res.* 17:31–63

Wohletz KH, Sheridan MF, Brown WK. 1989. Particle size distributions and the sequential fragmentation/transport theory applied to volcanic ash. *J. Geophys. Res.* 94(B11):15703–21

Wohletz K, Zimanowski B, Bütter R. 2013. Magma-water interactions. See Fagents et al. 2013, pp. 230–57

Woods AW. 2013. Sustained explosive activity: volcanic eruption columns and Hawaiian fountains. See Fagents et al. 2013, pp. 153–72

Wright HMN, Cashman KV, Gottesfeld EH, Roberts JJ. 2009. Pore structure of volcanic clasts: measurements of permeability and electrical conductivity. *Earth Planet. Sci. Lett.* 280:93–104

Wright HMN, Weinberg RF. 2009. Strain localization in vesicular magma: implications for rheology and fragmentation. *Geology* 37:1023–26

Yew CH, Taylor PA. 1994. A thermodynamics theory of dynamic fragmentation. *Int. J. Impact Eng.* 15:385–94

Zhang YX. 1998. Mechanical and phase equilibria in inclusion-host systems. *Earth Planet. Sci. Lett.* 157:209–22

Zhang YX. 1999. A criterion for the fragmentation of bubbly magma based on brittle failure theory. *Nature* 402:648–50

Annual Review
of Earth and
Planetary Sciences
Volume 43, 2015

Contents

Indexes

Errata

An online log of corrections to *Annual Review of Earth and Planetary Sciences* articles may be found at http://www.annualreviews.org/errata/earth